Plasma Losses in a Toroidal Theta Pinch with Superposed Helical Hexapole (n=4/3)

by

W. L o t z

IPP 1/92 November 1968

INSTITUT FÜR PLASMAPHYSIK

GARCHING BEI MÜNCHEN

INSTITUT FÜR PLASMAPHYSIK

GARCHING BEI MÜNCHEN

Plasma Losses in a Toroidal Theta Pinch with Superposed Helical Hexapole (n=4/3)

by

W. L o t z

IPP 1/92 November 1968

Die nachstehende Arbeit wurde im Rahmen des Vertrages zwischen dem Institut für Plasmaphysik GmbH und der Europäischen Atomgemeinschaft über die Zusammenarbeit auf dem Gebiete der Plasmaphysik durchgeführt.

IPP 1/92 W. L o t z

Plasma Losses in a Toroidal Theta Pinch with Superposed Helical Hexapole (n = 4/3) (in English)

November 1968

Abstract

A toroidal theta pinch discharge with superposed helical hexapole field is investigated. The characteristic data of the discharge are the same as reported in IPP 1/82: major diameter 52 cm, minor inner diameter of the vacuum vessel 6.0 cm, maximum theta pinch field between 10.5 and 21 kG, rise time (quarter cycle) 3.0 µs, maximum temperature between 40 and 100 eV, maximum density between 1 and 3 x 10^{16} cm^{-3}, minimum plasma radii between 0.5 and 1.0 cm, beta values between 0.3 and 1.0. The pitch-angle between a hexapole wire and the minor axis is 11^{o}, thus a hexapole wire passes 4/3-times around the minor axis when circling around the major axis once (the rotational number n equals 4/3). Plasma temperature, density, and radius turned out to be approximately the same as in the non-helical case. The plasma loss rates are determined by measuring the particle density; on the mean they are (34± 10)% smaller than those with non-helical hexapole and are virtually independent of the combination of parameters used. Within experimental error, the losses can be described as cusp losses with a cusp slit width of 0.54 ion gyro radii or as resistive losses with a diffusion coefficient 1.7 times the classical value. Bohm diffusion is not consistent with the measurements, the losses are up to 5 times smaller than those predicted by the Bohm formula. The machine is being converted to a fast Stellarator with higher helical pitch (pitch-angle 21^{o}, rotational number n = 8/3), thus the diameter of the (vacuum-field) separatrix will be doubled for the same value of the hexapole current and will be of the order of the plasma diameter.

I. Introduction

The plasma losses in a toroidal theta pinch with superposed non-helical hexapole field have been investigated in a previous report.[1] The losses could be accounted for by cusp losses assuming a cusp slit width of 0.8 ion gyro radii. Bohm diffusion was of the same order of magnitude but the thus predicted losses were up to three times higher than the measured ones. Classical (resistive) diffusion was too slow to be of significance at the temperatures measured.

All field lines of a non-helical hexapole field superposed in vacuo on a pure toroidal field (parallel to the minor axis) will eventually penetrate the wall of the vacuum vessel, provided the hexapole conductors are outside the vessel. If, instead, we use a helical hexapole, then there will arise a region near the minor axis of the torus, where the field lines (in vacuo) form magnetic surfaces and do not penetrate the wall of the vessel. The area of this region depends on the helical pitch given to the hexapole windings and on the ratio of the theta pinch-coil current to hexapole current. The line (or rather the surface) separating this inner region of closed surfaces from the outer "open-ended" region, is called the "separatrix".

II. Theory

A fast Stellarator is defined as an essentially toroidal device with the following properties:

a) There are nested magnetic surfaces inside the vacuum vessel that do not enclose an inner conductor.

b) The magnetic field has rotational transform, which is caused mainly by outer coils. A net toroidal current in the plasma is allowed, but usually this current is assumed to be zero and its contribution to the rotational transform is neglected.

c) The plasma is heated preferentially by fast rising magnetic fields, thus the beta-value will be relatively high. High beta is defined here as the region between approximately 0.1 and 1.

Recently Blank, Grad, and Weitzner [2] have shown theoretically in the large aspect ratio approximation, that a fast Stellarator with piecewise constant pressure could probably have favorable properties with respect to equilibrium and stability. Though it is not quite clear whether a continuous pressure distribution will be unstable or not, the authors are optimistic about the feasibility of a fast Stellarator with simple helical windings. They give an explicit expression for the approximate contour of a magnetic surface that separates two constant pressure regions; there should exist a whole series of nested magnetic surfaces.

To describe the results, we assume a torus with major radius R_o. A surface of approximately circular cross section with minor radius r_p contains the plasma at a constant pressure. On a toroidal surface with minor radius r_ℓ are wound 2ℓ wires ($\ell \geq 3$) with mean period h, helical number $k = 2\pi/h$, and rotational number $n = 2\pi R_o/h = k R_o$. The product $\ell \cdot n$ is an integer. If θ is the angular coordinate perpendicular to the minor axis and φ the angular coordinate parallel to the minor axis, then the coordinates θ_w and φ_w of one of the 2ℓ wires vary as $\theta_w = \varphi_w + m\pi/\ell$, $m = 0, 1, 2, \ldots, 2\ell-1$.

According to Ref. 2 the equation for the toroidal free boundary plasma interface is

$$r(\theta,\varphi) = r_p \left\{ 1 - a \cos (\ell\theta - \ell n \varphi) - b \cos\theta \right\} . \qquad (1)$$

The helical distortion, a cos $(\ell\theta - \ell n\varphi)$, is the result that would be obtained for the equivalent free boundary problem in a straight geometry. The toroidal perturbation, b cos θ, represents an inward displacement of the plasma (in the direction towards the major axis). Eq. (1) is an approximation for large aspect ratios, that is $R_o/r \gg 1$.

Constants a and b of eq. (1) are

$$a = \frac{C}{\ell k\, r_p (1 - \beta/2)} , \quad b = \frac{r_p\,(1 - \beta/2)}{R_o\,(\ell - 1)\,C^2} , \qquad (2)$$

where the constant C is the ratio of the helical field at $r = r_p$ to the toroidal field B_o at the minor axis $R = R_o$ (both in vacuum). For $\ell k\, r_\ell \ll 1$ constant C can be written

$$C \approx 2\ell q_I \left(\frac{r_p}{r_\ell}\right)^{\ell-1} , \quad q_I = \frac{I_\ell}{I_\theta} = \frac{\mu_o I_\ell}{2\pi r_\ell B_o} , \qquad (3)$$

I_ℓ is the helical current of one of the 2ℓ wires, I_θ is the theta current in an axial length $2\pi r_\ell$, and q_I, thus, is a measure of the ratio of the helical current to the theta current.

For $\ell = 3$ (hexapole) constants a and b can be written

$$a = \frac{2\, r_p\, q_I}{r_\ell^2 k\,(1 - \beta/2)} , \quad b = \frac{r_\ell^4\,(1 - \beta/2)}{72\, r_p^3\, R_o\, q_I^2} . \qquad (4)$$

The helical distortion a is proportional to the current ratio q_I and the plasma radius r_p, it increases weakly with β. The toroidal displacement b is inversely proportional to q_I^2 and to r_p^3 (which at least for $\beta = 0$ is in contradiction to numerical calculations, see below), b decreases a bit with increasing β.

Let us now have a look at the case $\beta = 0$, for which eqs. (4) can be written

$$a = \frac{2\, r_p\, q_I}{r_\ell^2 k} , \qquad b = \frac{r_\ell^4}{72\, r_p^3\, R_o\, q_I^2} . \qquad (5)$$

The validity of eq. (1) clearly is restricted to values of constants a and b smaller than unity, because $r(\theta, \varphi)$ cannot be negative. The magnitude of the helical distortion is further limited by the separatrix, which for $\ell = 3$ is a triangle. A symmetric triangle with inner radius $2\, r_p/3$ and outer radius $4\, r_p/3$ can be approximated with eq. (1) by $a = 1/3$. $a < 1/3$ gives an upper limit to r_p in eq. (5):

$$r_p < \frac{r_\ell^2 k}{6\, q_I} \approx \frac{d_s}{2} , \qquad (6)$$

d_s is the diameter of the separatrix.

The center of the nearly circular surface according to eq. (1) is at

$$R_c = R_o - r_c , \qquad r_c = b\, r_p = \frac{r_\ell^4}{72\, r_p^2\, R_o\, q_I^2} . \tag{7}$$

r_c thus should be inversely proportional to r_p^2. This is in contradiction to numerical calculations,[3] the results of which we give in Figs. 3 to 6. As can be verified very easily with a pair of dividers, r_c is independent of r_p and of q_I within drawing accuracy. We must conclude, therefore, that eq. (2) is not correct as far as constant b is concerned and that no lower limit for r_p can be derived by applying the inequality $b < 1$, as has been done in Ref. 2.

Nevertheless, even for $\beta = 0$ there is a lower limit to r_p. In fact, numerical calculations [3,4] show that generally there exists an "inner separatrix", which has been indicated in Fig. 3 . This "inner separatrix" separates two "nests" of magnetic surfaces near the minor axis and the rotational transform on this inner separatrix is zero! The inner separatrix intersects the axis $z = 0$ at three points, which can be seen in Fig. 7 for configuration I. Inside the inner separatrix the rotational transform is very low and plasma of finite resistivity could certainly not be in equilibrium if it were restricted to this inner region of low rotational transform.

We have seen that according to Ref. 2 the magnetic field configuration should not depend sensitively on β, though the stability of the plasma column is questionable when β approaches 1. The magnetic field configuration at high β should be similar to the vacuum field. Blank, Grad, and Weitzner are hopeful that a fast Stellarator could have favorable properties with respect to equilibrium and stability. At least their free boundary step function equilibrium[2] exists under a wide range of parametric values, they found many different indications of MHD stability of the device and none to the contrary. The question remains, if the approximation of a continuous pressure profile by a step function (which leads to stability) is a reasonable approximation.

In the approximation of Blank, Grad, and Weitzner, the plasma is assumed to have infinite conductivity, such that electrical fields parallel to magnetic field lines cannot exist. Thus an electrical field produced by a gradient in the magnetic field will be cancelled if there is a finite rotational transform of the magnetic field. In a plasma with finite conductivity, the cancellation of electrical fields will be the better, the higher the rotational transform is. At given radius $r_p \ll r_\ell$ the rotational transform is proportional to C^2/k (in vacuo), as can be verified in Fig. 7.

It is clear that the plasma should be inside the (outer) separatrix, otherwise the plasma surface would not be a closed magnetic surface and part of the plasma would be lost along magnetic field lines to the wall. According to eq. (6), the diameter, d_s, of the separatrix is proportional to k/q_I (for $d_s \ll 2r_\ell$, $\ell = 3$).

Thus, to overcome the wellknown torus drift [5] we need high enough rotational transform, and to overcome cusp losses [1] we need a large enough diameter of the (outer) separatrix. The problem of plasma instabilities will be more severe in an M+S-like configuration [6] than in a fast Stellarator and will be neglected for the following; certain low-beta Stellarators (with continuous pressure distribution) are supposed to be MHD-stable.

III. Configuration Parameters

A Stellarator field can be characterized by the following interdependent parameters:

1) multiplicity ℓ of the multipole wires,
2) helical number k or rotational number n of the multipole wires,
3) area or diameter of the (outer) separatrix,
4) rotational transform versus minor radius,
5) well depth.

In order to be able to compare our experimental results with previous measurements on a non-helical hexapole, we chose $\ell = 3$ (Fig.1). The rotational number n could not be varied arbitrarily but had to be adapted to the possibilities of the devise SPINNE. The smallest possible rotational number greater than zero was $n = 4/3$, which is equivalent to a pitch angle of 11°, a helical period $h = 122$ cm, and a helical number $k = 0.05\ cm^{-1}$. Further possibilities are $n = 8/3$, $n = 12/3$, etc. (Fig.2).

The (outer) separatrix is defined as the line or rather the surface that separates the inner region of closed nested flux surfaces from the outer cusp region (where all field lines eventually hit the wall of the vacuum vessel). Plasma in the outer region will be lost by escaping along magnetic field lines, while plasma inside the separatrix has a chance to compensate the still present magnetic field gradient by charge transfer along magnetic field lines with rotational transform. Inside the separatrix a field line with absolute (non-zero) minimum magnetic field would be most desirable, but is not possible in a vacuum field; local minima inside the separatrix are not excluded. In low-beta theories average-minimum-B configurations are considered.

In the case of a helical hexapole ($\ell = 3$), the separatrix (in vacuo) is triangularly-shaped, its cross-sectional area is the larger the larger the pitch of the helical windings and the lower the ratio of hexapole current to theta pinch-coil current is (eq.6). In the limiting case of no hexapole current, all magnetic field lines inside the (axissymmetric) vacuum vessel stay inside, but then we have no rotational transform and the wellknown torus drift results.[5] The problem is, to compromise between too large a separatrix area with relatively small rotational transform and torus drift, and too small a separatrix area with resulting cusp losses. Probably the separatrix diameter (in vacuo) should be of the order of the plasma diameter.

A given cross-sectional area of the separatrix (in vacuo) at given theta-pinch-coil current can be achieved in two different ways: either high helical pitch plus high hexapole current (and high rotational transform), or lower helical pitch plus proportionally lower hexapole current (and proportionally lower rotational transform). If an absolute minimum of the magnetic field inside the vacuum vessel or even inside the separatrix should be necessary, then the hexapole current must exceed a certain minimum value in order to compensate the field gradient of the torus field B_{φ}. In our experiments with non-helical hexapole,[1] this absolute minimum was essential for equilibrium, because the cross-sectional area of the separatrix was zero. On the other hand, the hexapole current should be as low as possible for technical and economical reasons.

Therefore, we started our experiments with a relatively low pitch, varying the hexapole current by a factor of two. In configuration I (Table I) we had a separatrix diameter of about 0.8 cm, while this diameter increased to about 1.6 cm in configuration II (in vacuo). The rotational transform of configuration II was only one fourth that of configuration I at given radius, but about the same near the separatrix, (naturally at different radii, Fig. 7).

Future experiments (configurations III and IV) will have twice the pitch with about doubled separatrix diameter at the same hexapole current. We will then be able to compare experiments with equal separatrix diameter but different rotational transform; the rotational transform of configuration III is about twice as high as that of configuration II. Configuration IV will again give an even larger separatrix diameter at reduced rotational transform.

If multiplicity, rotational number, and current distribution are given, the other field parameters can be calculated. H. Welter, M. Croci, and H. Gorenflo [3] have done this for a vacuum magnetic field of a helical hexapole with rotational numbers $n = 4/3$ and $n = 8/3$ with superposed toroidal field.

They took into account the approximate current distribution within the hexapole conductors (equal current in each of the 36 wires, Fig. 1), but the influence of the theta pinch coil on the field configuration inside the vacuum vessel has been neglected. The ratio of hexapole current to theta-pinch-coil current was adjusted during calculations in such a way that the experimental ratio of hexapole field to toroidal field was simulated. This means that the hexapole current in the actual experiment is higher than in the calculations (compared to the theta pinch-coil current), because the hexapole field is weakend by mirror currents in the theta pinch-coil.

Neglecting these mirror currents during calculations should have no serious influence on the field configuration near the minor axis, as their first order effect is a decrease in magnetic field strength by a constant fraction independent of radius. Near the hexapole wires, and especially between the hexapole wires and the theta-pinch coil, the influence of the mirror currents is drastic, but this region is of no interest here. Near the minor axis the influence of a high-beta plasma on the magnetic field configuration most probably will be by far higher than the influence of the neglected mirror currents.

In the experiment we vary the theta-pinch-coil current and the hexapole current by varying the respective bank voltages (main bank and hexapole bank). Table I gives a connection between calculated configurations I, II, III, and IV and bank voltages used. Configurations I and II have the same rotational number and so do configurations III and IV. With configurations I and III the magnetic field strengths of the hexapole field B_r and the toroidal field B_φ are approximately equal at a point halfway between two hexapole conductors. Configurations II and IV have only half the hexapole bank voltage, half the hexapole current, and half the hexapole magnetic field strength. Configuration Ia is intermediate between configuration I and II, but closer to configuration I. Configuration Ia had to be used, in order to spare the hexapole wires at higher bank energy level.

The results of the vacuum-field calculations are shown in Figs. 3 to 6 in the form of magnetic flux surfaces, while Fig. 7 gives the rotational transform versus the radius along the horizontal center line ($z = 0$) of Figs. 3 to 6. The separatrix proper is not shown in Figs. 4 to 7, it is situated very close to the last flux surface shown. Configurations II and III in fact have nearly the same flux surfaces and the same separatrix, but they differ in their rotational transform by approximately a factor of two. The

inner separatrix is shown approximately in Fig. 3b, it is very similar in form and size (allowing for different scaling factors) for the configurations II to IV shown in Figs. 4 to 6, seemingly it does not depend on k or q_I very much.

In Figs. 8 to 10 the vacuum magnetic field strengths are given versus the major radius for a diameter passing between two hexapole conductors, normalized to the toroidal field at R_o = 26 cm. The hexapole conductors are at r_ℓ = 3.75 cm. In cases I and III the absolute minimum in the resulting field strength is near R = 27 cm, while in cases II and IV this minimum is near R = 28 cm (case Ia is intermediate). In cases I and II this minimum is well outside the separatrix, while in cases III and IV both are closer together.

If we define an absolute well-depth W as the difference of the field strengths at R = 29 cm (between hexapole conductors) and the minimum field, divided by the minimum field:

$$W = \frac{B_{29} - B_{min}}{B_{min}} ,$$

we get $W_I = W_{III} = 30\ \%$, $W_{Ia} = 18\ \%$, $W_{II} = W_{IV} = 5\ \%$.

If we define an average well depth w

$$w = \frac{\bar{q}(r) - \bar{q}(0)}{\bar{q}(0)}$$

with $\bar{q}$ being a mean value of q on a magnetic surface,

$$q = \int \frac{ds}{B} ,$$

we get for r = 1 cm the following extrapolated values from the calculations of Welter, Croci, and Gorenflo: [3] $w_I = 0.20\ \%$, $w_{II} = 0.35\ \%$, $w_{III} = 0.23\ \%$, and $w_{IV} = 0.34\ \%$. Within the accuracy of the calculations all four average well depths can be set equal to 0.3 %, which means that all four configurations, I through IV, have the same nominal average well depth of relatively low magnitude (in vacuo).

In Table I we have calculated the constants of eqs. (1) to (6) in order to compare the theoretical parameters of Blank, Grad, and Weitzner with the parameters used in the experiments. The helical distortion, a, is always smaller than one (but not smaller than 1/3), assuming r_p = 1 cm and β = 0.5. This helical distortion will be smaller for our future configurations III and IV. The toroidal distortion, b, taken from eq. (4), is not smaller than one; but, as has been shown above, the validity of eq. (4) with respect to b is questionable.

IV. Experiments

The SPINNE device is a toroidal theta pinch with major radius R_o = 26 cm. The vacuum vessel is made of pyrex glass and has a minor inner radius r_o = 3.0 cm , while the theta-pinch coil has a minor inner radius r_θ = 4.6 cm . Between the vacuum vessel (minor outer radius 3.5 cm) and the coil there are additional conductors (minor radius r_ℓ = 3.75 cm) producing the helical hexapole field. There are six conductors, each consisting of six single wires (Fig. 1). The angle between a wire and a line parallel to the minor axis (pitch-angle) is 11° on the average. In a toroidal coordinate system (r,θ,φ) the coordinate θ_w of a wire increases linearly with φ_w : $\theta_w = n\varphi_w$ + const. Thus a hexapole wire passes 4/3-times around the minor axis when circling around the major axis once (the rotational number n equals 4/3). A picture of the hexapole windings before immersion in silicone rubber is given in Fig. 2a for n = 4/3 (present experiments) and in Fig. 2b for n = 8/3 (future experiments).

Some data of the discharge circuits are given in Table II, which are essentially the same as in Ref. 1. Each circuit is crowbarred (Fig. 11) and its energy is characterized by the voltage to which the capacitor bank is charged. Both circuits have approximately the same discharge frequency and are fired nearly at the same time. The hexapole current usually begins with a time lag of a few hundred nanoseconds compared to the theta-pinch current, in order not to interfere with the theta pinch heating by rapid implosion.

Eight sets of parameters were investigated (Table III): we varied the filling pressure of hydrogen (40, 30, and 20 mTorr) at a given bank voltage, and we varied the bank voltage at a given filling pressure of 20 mTorr hydrogen. Experiments (1) to (5) are nearly identical in their parameters with those of Ref. 1; experiments (6) to (8) were added, in order to compare configuration I (or Ia) with configuration II.

We tried to obtain the plasma radius by photometric evaluation of streak pictures in integral light as described in Ref. 1 (Fig. 12). We used a film with higher speed (Kodak 2485) and developed in Neofin Rot in order to combine high speed and wide exposure range (the recommended developer Kodak MX-642 gave higher speed but only a factor of 8 in range with rather low resolution; Agfa Scopix G was less sensitive by a factor of 2, Agfa Record by a factor of 4). The gain in film speed nevertheless was not high enough to allow the use of filters for suppressing line radiation, but we were able to improve the time resolution by a factor of two and got denser exposures. The time resolution then was about 0.25 µs.

Though circumstances seemed to be more favourable, our streak pictures turned out to be useless, because of bright luminiscence halfway between the adjacent hexapole conductors. In order to get more information from plasma otherwise hidden behind these hexapole conductors, we had widened the gap between conductors at the position of the streak slit. At this position the magnetic field near the wall was of course not as strong as at all other points around the torus and the plasma most probably hit the wall preferably at this viewing port.

We were forced, therefore, to use the plasma radii of Ref. 1 for the non-helical hexapole case also for the helical hexapole. The results are not unreasonable, though certain discrepancies in the line density must be attributed to these not quite exact plasma radii. Anyway, after maximum compression at 3 µs after the start of the main discharge, the plasma radius is nearly constant for the non-helical case as well as for the helical case and thus uncertainties in plasma radius are of minor importance after t = 3 µs.

The mean electron densities n_e calculated with the plasma radii of Ref. 1, are given in Fig. 13. They are derived in the same way as in Ref. 1, viewing parallel to the plane of the torus through an opening in a hexapole conductor. The observed luminescence between hexapole conductors has not influenced these measurements, because light from those parts of the vacuum vessel could not enter the spectrograph.

Electron temperatures were derived in the same way as in Ref. 1. Within experimental error the measured temperatures were identical with those of Ref. 1 and are not reproduced in this report. Also impurity levels, beta values, and relaxation times are essentially the same as in Ref. 1.

V. Discussion

In Figs. 14 to 21 the measured line densities are given for the eight different experiments together with a best fit straight line in order to evaluate the experimental loss rate. For comparison, the measured line densities of Ref. 1 are indicated. The line density is $N = \pi r_p^2 n_e$ with the plasma radius r_p taken from the respective experiments of Ref. 1. The minimum in line density for times near $t = 2$ µs must be attributed to differences in the actual plasma radius between the non-helical and the helical case or to movements of the plasma. Therefore, the loss rate indicated for each graph has a higher probable error of appr. $^{+40}_{-30}$ %.

The loss rates are summarized in Table III. If we take the mean value of experiments (1) to (5) we get $2.14 \times 10^5\ s^{-1}$ for the case $n = 0$ and $1.42 \times 10^5\ s^{-1}$ for $n = 4/3$, or a decrease in loss rate by (34 ± 10) %. Within experimental error, the loss rates of $n = 4/3$ are independent of the combination of parameters used; even configuration II does not give a markedly different loss rate, though the diameter of the vacuum field separatrix is twice as large (the well depth W is appreciably smaller, the rotational transform at constant r is only 1/4).

In Fig. 22 we compare the measured loss rates with the anticipated losses from a line cusp. Within experimental error the measured losses can be represented by line cusp losses with a slit width of 0.54 ion gyro radii, compared to 0.81 ion gyro radii for the case $n = 0$.

In Fig. 23 we compare the measured loss rates with the anticipated losses, assuming only classical (resistive) diffusion. For classical diffusion we took the formula derived in Ref. 1 for diffusion in a hexapole field, taking into account that in the outer regions the plasma can reach the wall along magnetic field lines. We took not into account enhanced diffusion caused by currents parallel to magnetic field lines with rotational transform. Within experimental error, the measured loss rates can be represented by resistive diffusion with a diffusion coefficient 1.7 times the classical value.

In Fig. 24 we compare the measured loss rates with the anticipated losses from Bohm diffusion, assuming a smooth boundary of the plasma with a thickness comparable to the plasma radius. We took not into account enhanced losses in the outer regions by plasma escaping along magnetic field lines. The measured losses clearly cannot be described by Bohm diffusion, the losses of experiment (5) are a factor of 5 below the expected value.

In Fig. 12 we show a streak picture of the plasma in experiment (5) both for $n = 0$ and and $n = 4/3$. In both cases the plasma drifts to the outer part of the vacuum vessel for the first microsecond after the beginning of the main discharge and is pushed back then by the rising hexapole field. After a few oscillations, it stays quiet in an equilibrium

position a bit off the minor axis in the direction of larger R before it diminishes there, while illuminating the wall of the vacuum vessel in a rather thin region halfway between hexapole wires. There is no indication of a shift towards the major axis as predicted by eq.(1). It seems that the equilibrium position is near the absolute minimum of the magnetic field, indicated in Fig. 8, which implies that most of the plasma will be outside the separatrix and can be lost along magnetic field lines.

The machine is now being converted to a rotational number n = 8/3 in order to test configurations III and IV. We hope to get another reduction in loss rates by approximately 30 % before we reach the limiting case of classical diffusion (Fig.23). As yet we were not able to observe gross plasma instabilities. If the case n = 8/3 should give favourable results, a larger toroidal machine could be built with higher temperatures. We still have to verify if and how much a possible net toroidal plasma current has altered the magnetic field configuration (and the rotational transform) and has possibly influenced the measured loss rates.

References

1) J.Junker and W. Lotz, Report IPP 1/82, Institut für Plasmaphysik, Garching bei München (1968).

2) A.A. Blank, H. Grad, H. Weitzner, Plasma Physics and Controlled Nuclear Fusion Research, Conference in Novosibirsk, 1.-7. Aug. 1968, paper CN-24/K-6.

3) H. Welter, M.G. Croci, H. Gorenflo, W. Lotz, Numerical calculations of vacuum fields in a $\ell = 3$ stellarator (with the help of our computer IBM 7090), not published. Results are given in Figs. 3 to 7 (1968).

4) A. Gibson, Phys. Fluids 10, 1553 (1967).

5) J. Junker, Phys. Fluids 11, 646 (1968).

6) W. Lotz, E. Remy, G.H. Wolf, Nucl.Fusion 4, 335 (1964).

Table I: Characteristic parameters of the vacuum field configurations. Configurations III and IV have not yet been realized experimentally. Constant C is taken from eq. (3), constants a and b from eqs. (4), assuming r_p = 1 cm and β = 0.5.

Configuration No.		I	Ia	II	III	IV
Rotational number n		4/3	4/3	4/3	8/3	8/3
Main bank voltage	(kV)	8	-	8	8	8
Hexapole bank voltage	(kV)	10	-	5	10	5
Main bank voltage	(kV)	-	12	12	-	-
Hexapole bank voltage	(kV)	-	12	7.5	-	-
Main bank voltage	(kV)	-	16	16	-	-
Hexapole bank voltage	(kV)	-	16	10	-	-
Diameter of the Separatrix	(cm)	0.8	1.0	1.6	1.6	2.9
Well depth W	(%)	30	18	5	30	5
Well depth w	(%)	0.3	0.3	0.3	0.3	0.3
Helical period h	(cm)	122	122	122	61	61
Helical number k	(cm^{-1})	0.05	0.05	0.05	0.1	0.1
Current ratio q_I		0.24	0.19	0.12	0.24	0.12
Constant C		0.10	0.08	0.05	0.10	0.05
Constant a		0.9	0.7	0.4	0.4	0.2
Constant b		1.4	2.3	5.8	1.4	5.8
Parameter ℓ k r_ℓ		0.6	0.6	0.6	1.1	1.1

Table II: Data of the batteries used.

Preionization Bank:

Energy	0.9	kJ
Voltage	25	kV
Capacitance	3	µF
Ringing frequency	700	kHz

Main Bank:

Energy	58	kJ
Voltage	18	kV
Capacitance	360	µF
Rise time $\tau/4$	3.0	µs
Magnetic field B_{max}	24	kG
Field rise $\dot{B}_o$	10^{10}	G/s
Crowbar time	30	µs

Hexapole Bank:

Energy	58	kJ
Voltage	18	kV
Capacitance	360	µF
Rise time $\tau/4$	2.9	µs
B_{max} at r = 3 cm*	16	kG
Crowbar time	30	µs

*between conductors.

Table III: Parameters of the experiments.

Experiment No.	(1)	(2)	(3)	(4)	(5)	(6)	(7)	(8)
Configuration No.	I	I	I	Ia	Ia	II	II	II
Main bank voltage (kV)	8	8	8	12	16	8	12	16
Hexapole bank voltage (kV)	10	10	10	12	16	5	7,5	10
Filling pressure (mTorr H_2)	40	30	20	20	20	20	20	20
$T_{e\ max}$ (eV)	38	50	62	76	93	62	76	93
$n_{e\ max}$ ($10^{16}/cm^3$)	1.7	1.6	1.5	2.1	2.8	1.2	1.6	2.6
$r_{p\ min}$ (cm)	0.95	0.86	0.80	0.60	0.46	-	-	-
Loss rate n = 4/3 (10^5/s)	1.4	1.3	1.6	1.5	1.3	1.4	1.7	1.6
n = 0 (10^5/s)	1.8	2.3	2.6	2.1	1.9	-	-	-

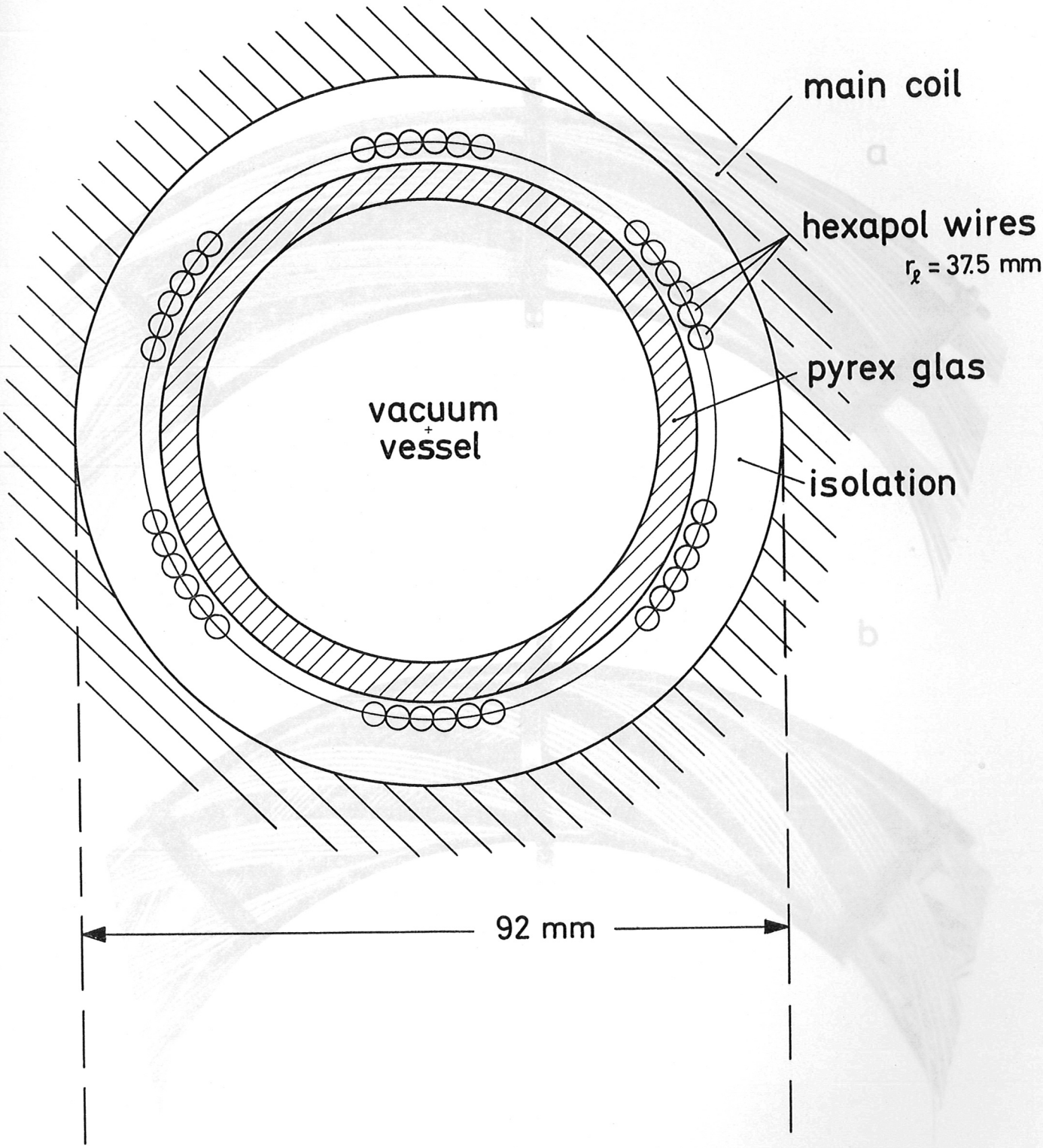

Fig. 1 Arrangement of vacuum vessel, hexapole conductors, and main coil. Each hexapole conductor consists of six single wires. The inner diameter of the vacuum vessel is 60 mm.

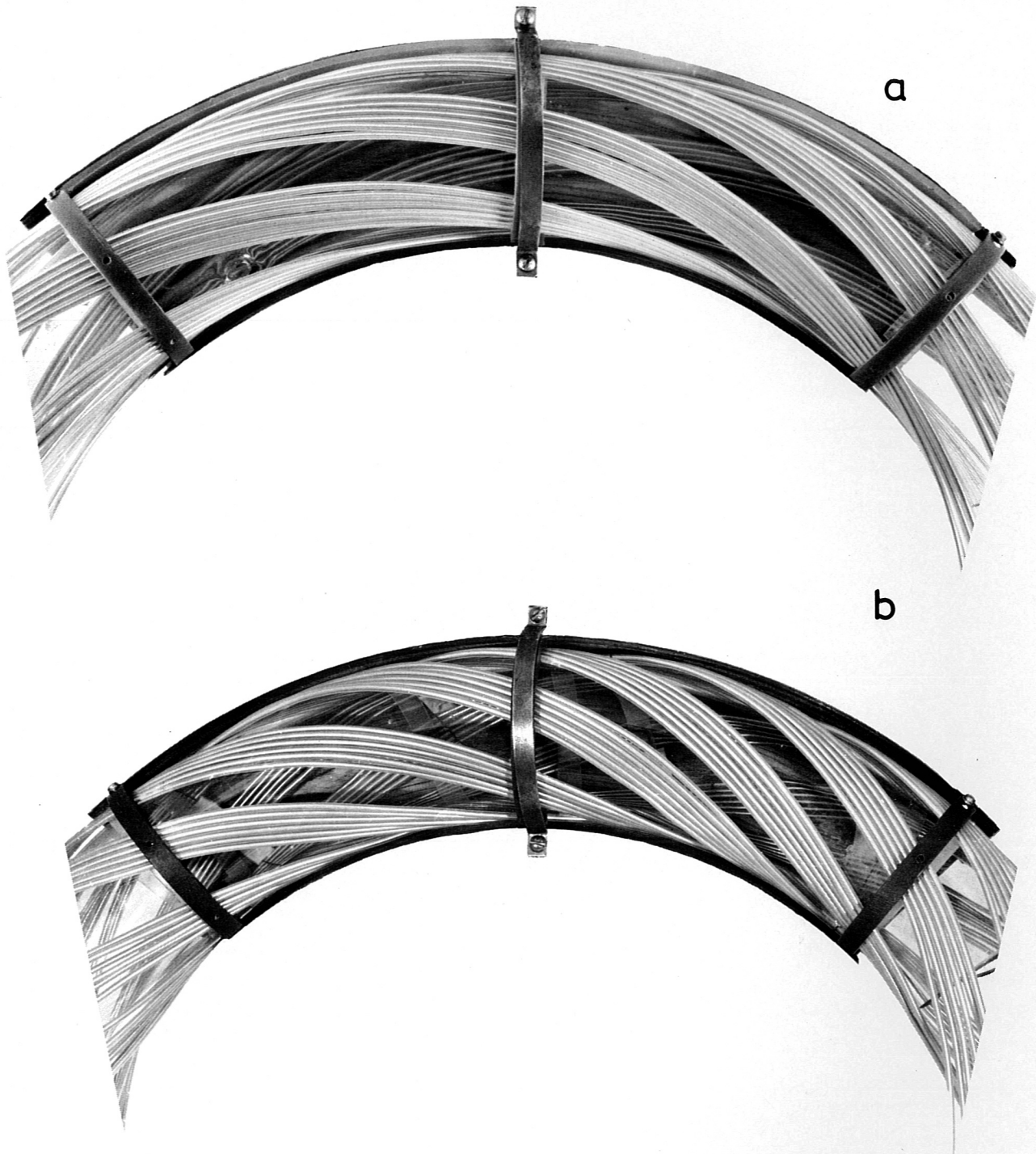

Fig. 2 Arrangement of hexapole wires on the surface of the vacuum vessel. These photographs have been taken before the silicone rubber had been applied.
a) rotational number n = 4/3, b) n = 8/3.

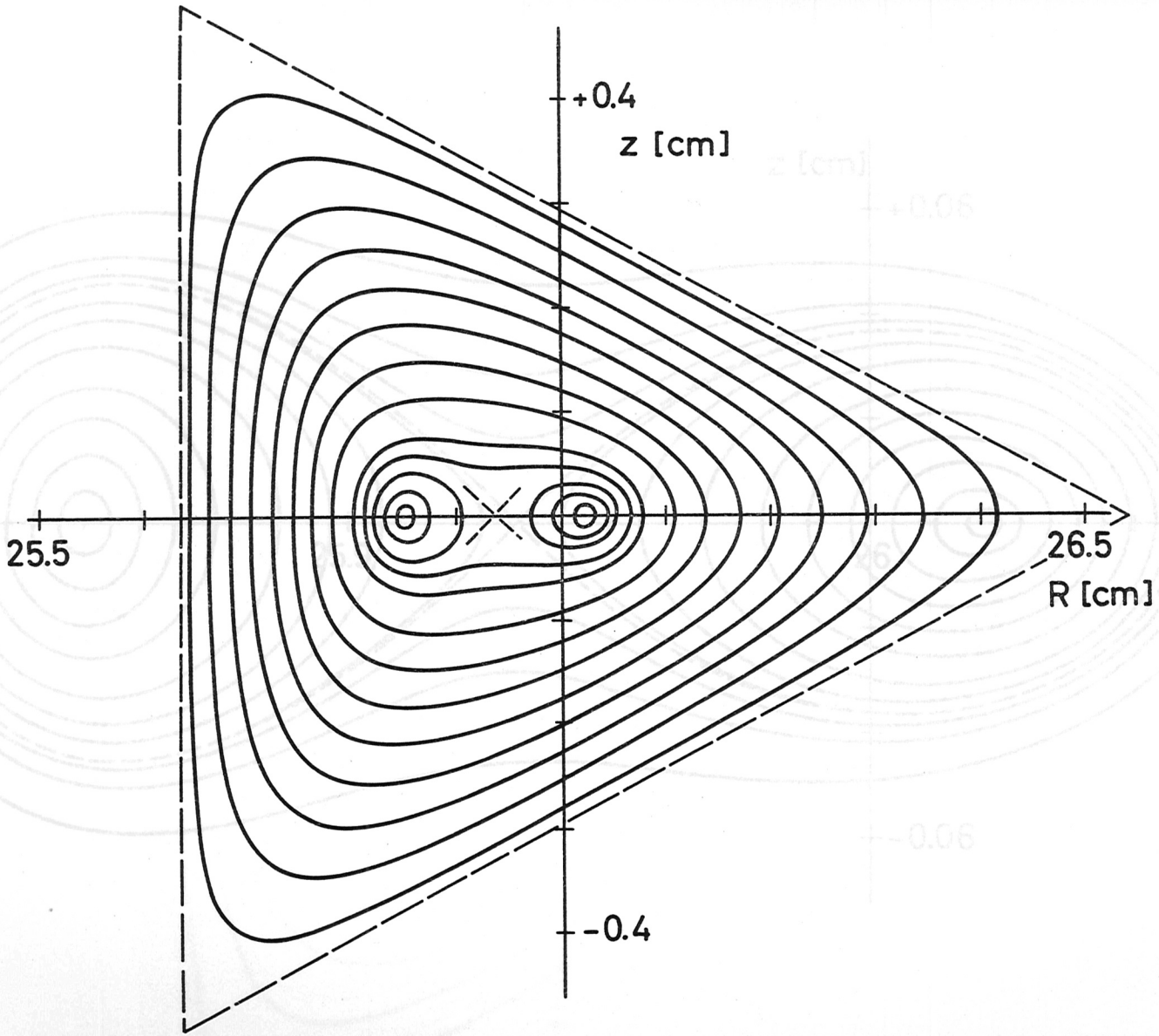

Fig. 3a Magnetic surfaces of configuration I. The (outer) separatrix is represented by a dashed curve, the approximate position of the inner separatrix is indicated by a dashed cross. For an enlarged reproduction of the center part, see Fig. 3b!

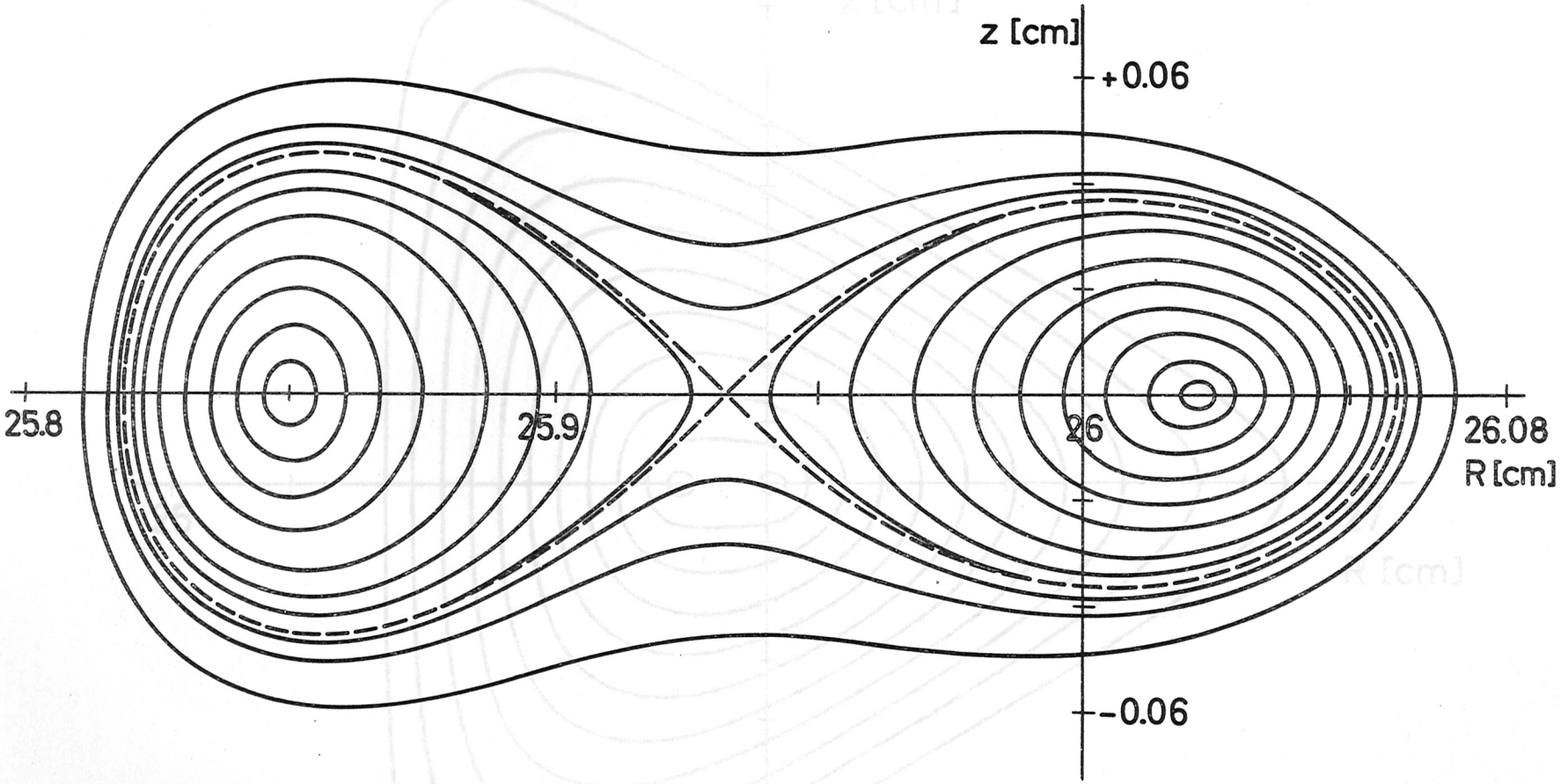

Fig. 3b Enlarged center part of Fig. 3a. The dashed curve represents the inner separatrix with zero rotational transform. This is configuration I.

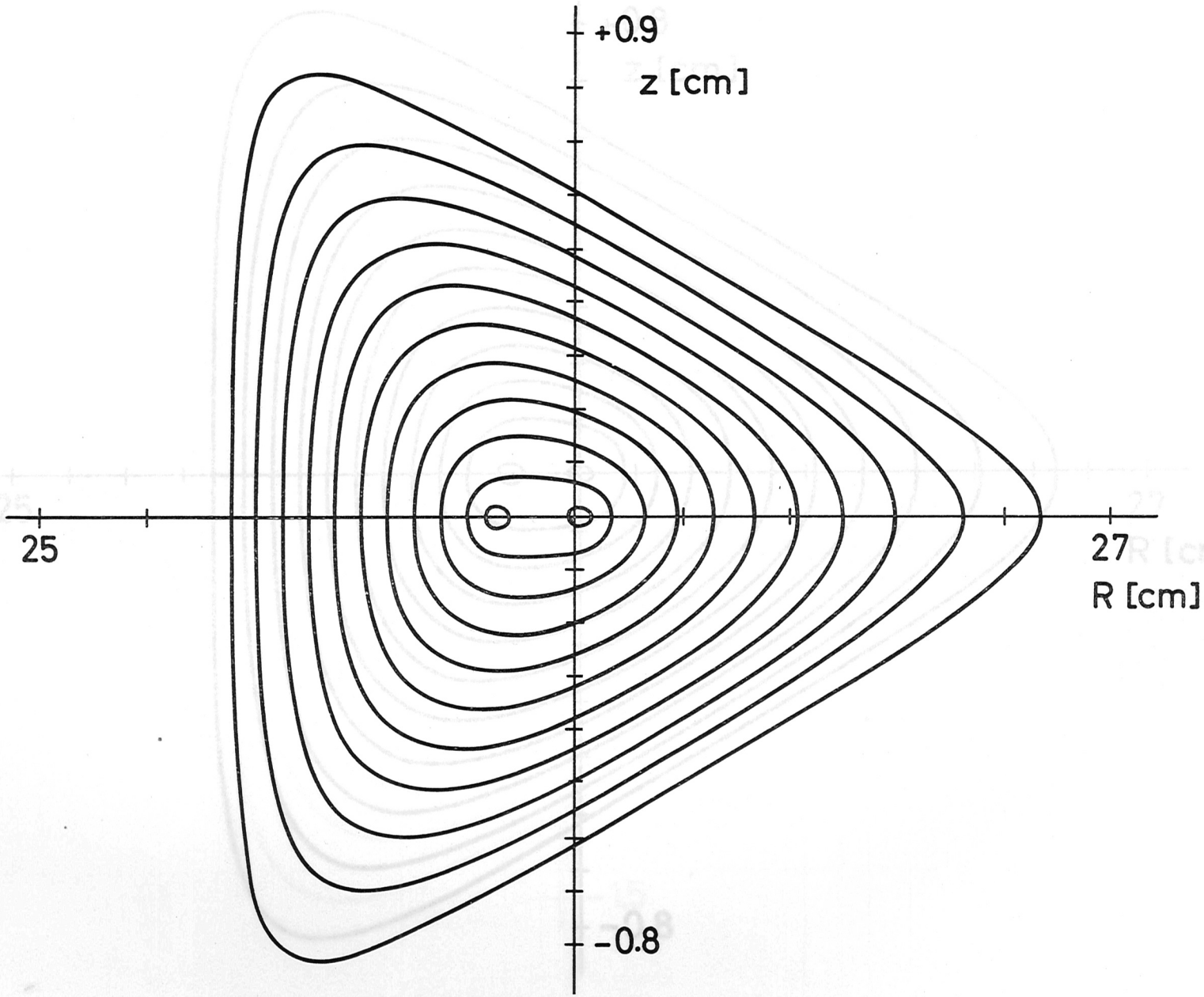

Fig. 4 Magnetic surfaces of configuration II. Note that Fig. 3 has a different scale!

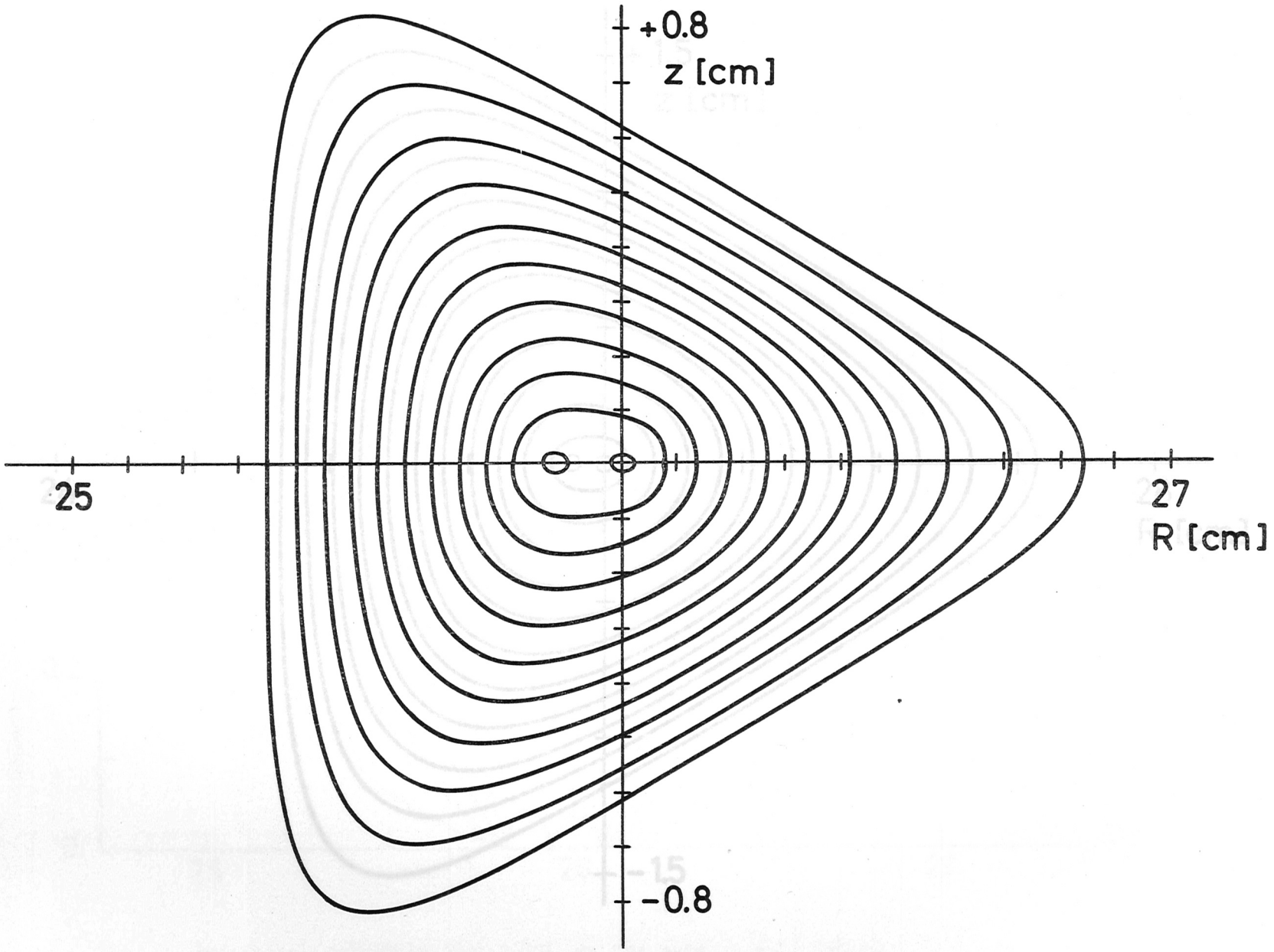

Fig. 5 Magnetic surfaces of configuration III.

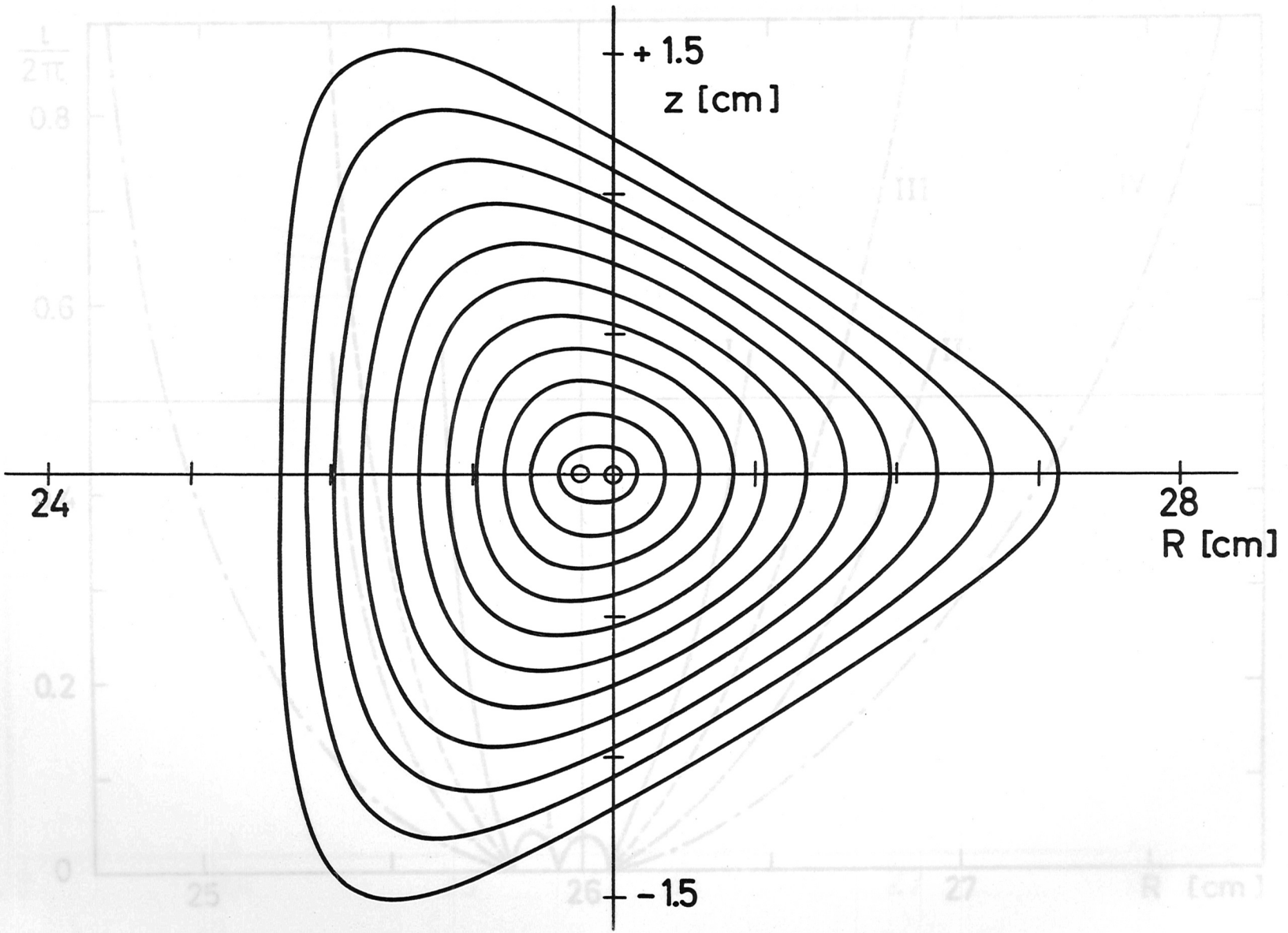

Fig. 6 Magnetic surfaces of configuration IV.

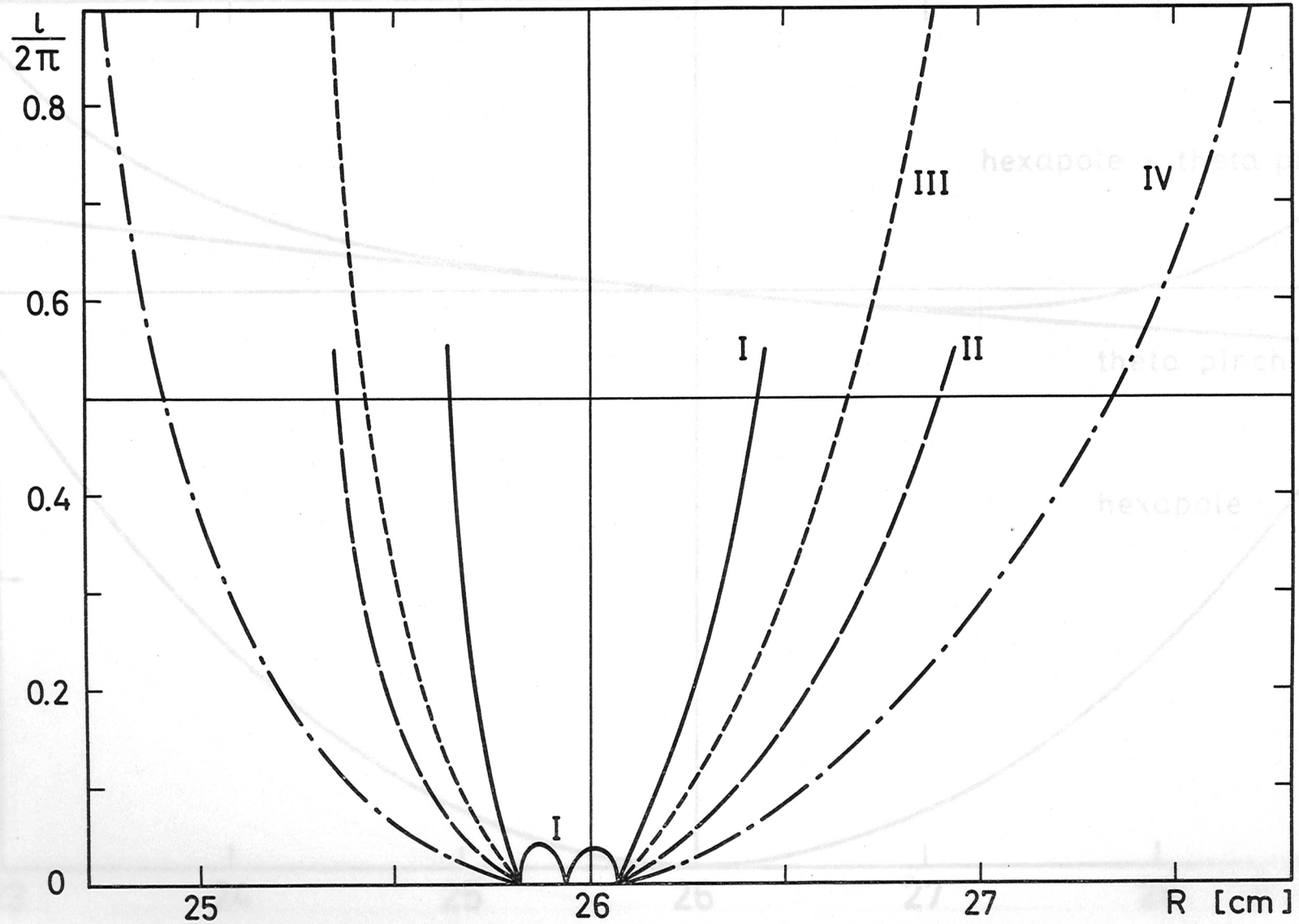

Fig. 7 Rotational transform $\iota = \iota/2\pi$ on the axis $z = 0$ (Figs. 3 to 6) versus major radius. In the center part, only configuration I is shown; the rotational transform of configurations II to IV is everywhere smaller than that of configuration I (within its outer separatrix).

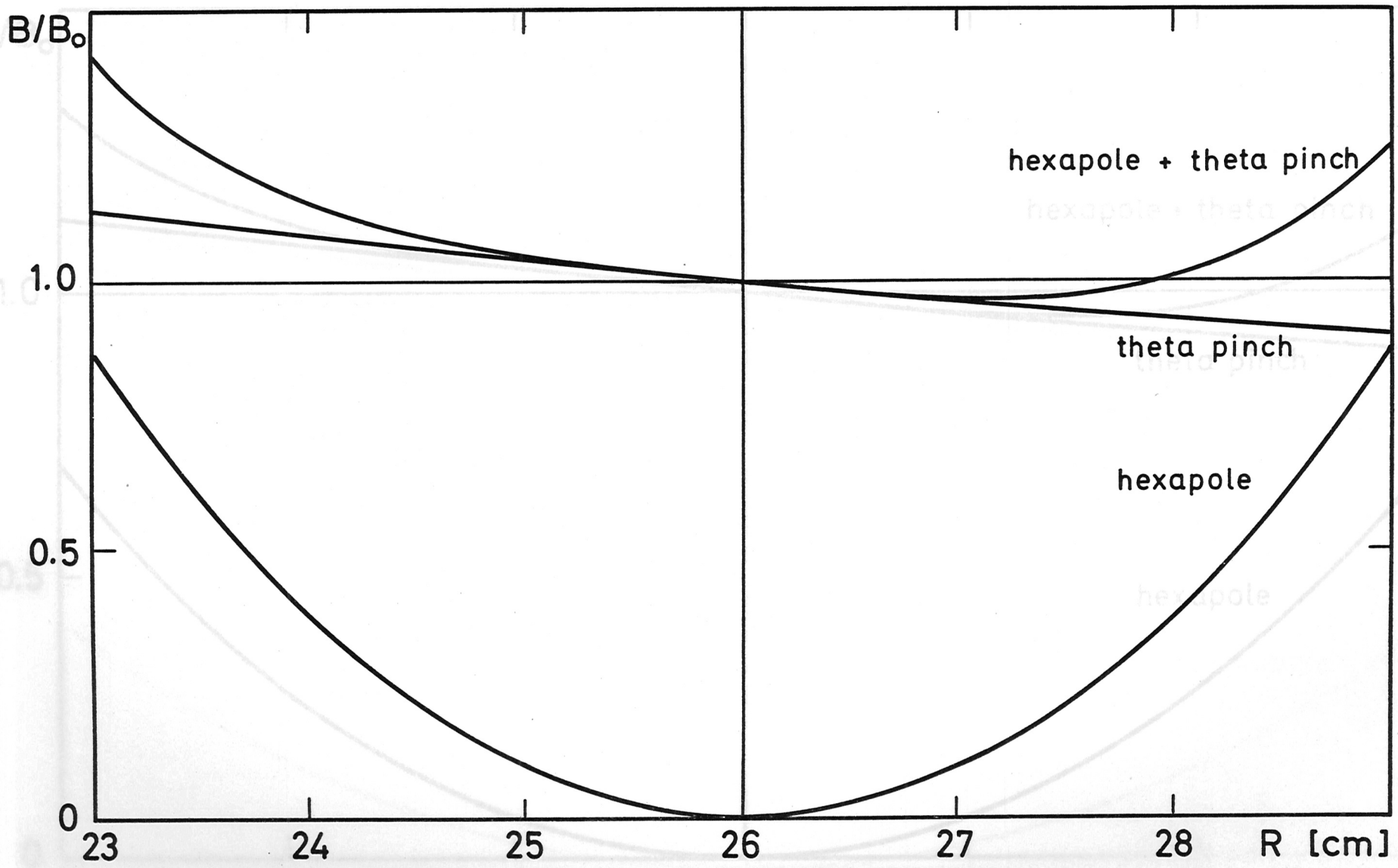

Fig. 8 Magnetic field strengths of hexapole and theta-pinch field normalized to B_o at $R = R_o$ for configurations I and III. The magnitude of the hexapole field is nearly independent of the rotational number n .

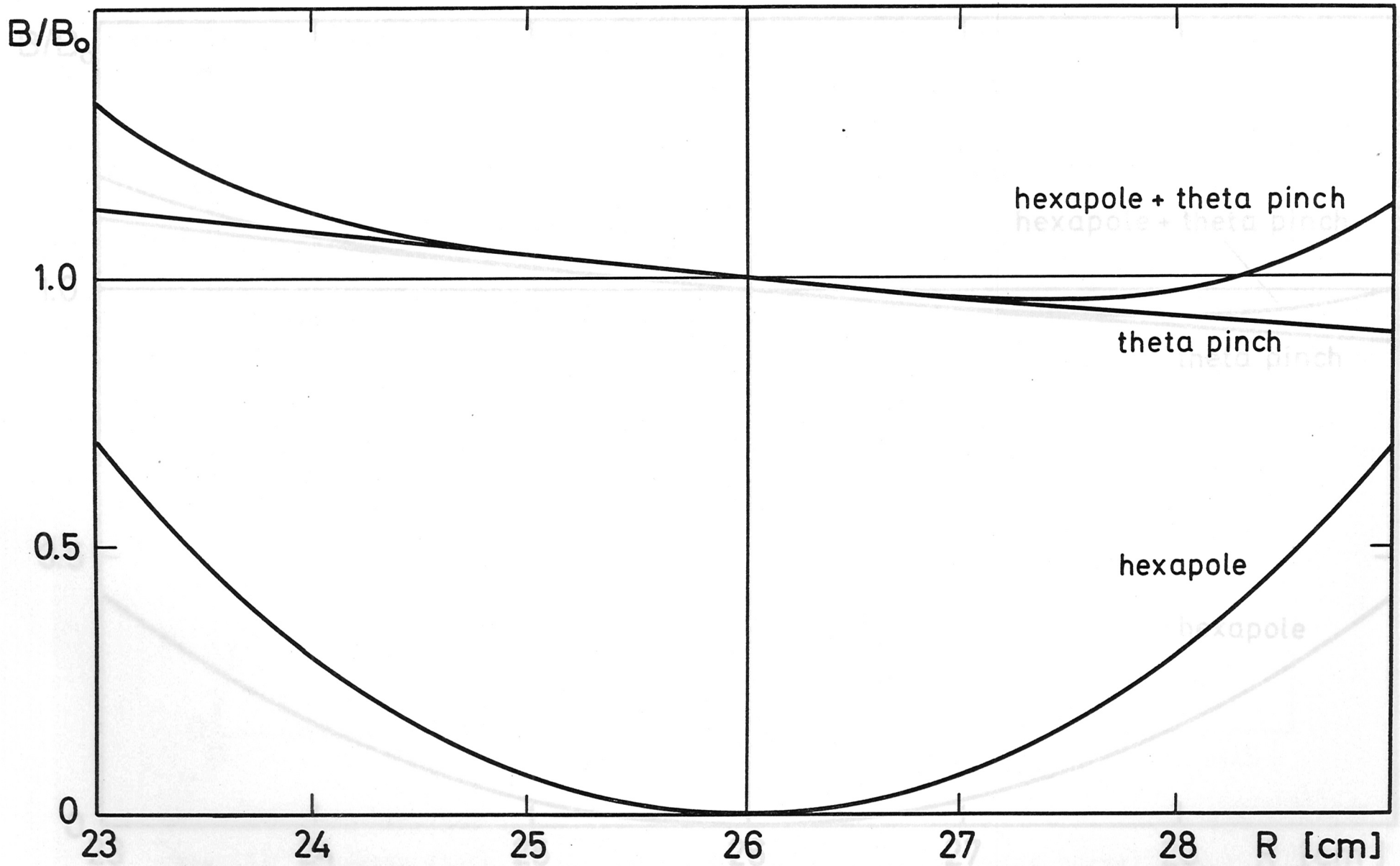

Fig. 9 Hexapole field and theta-pinch field of configuration Ia.

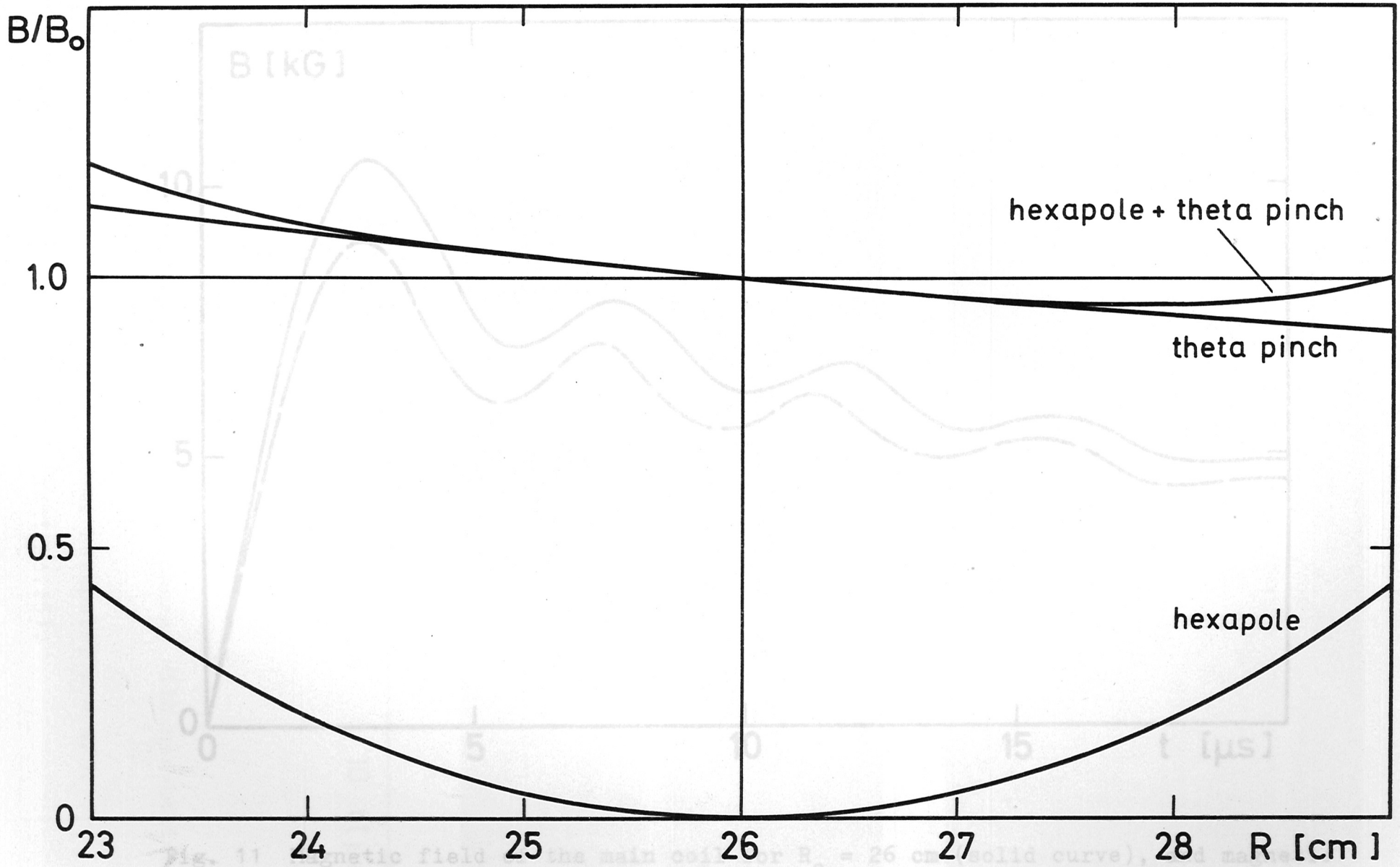

Fig. 10 Hexapole field and theta-pinch field of configurations II and IV.

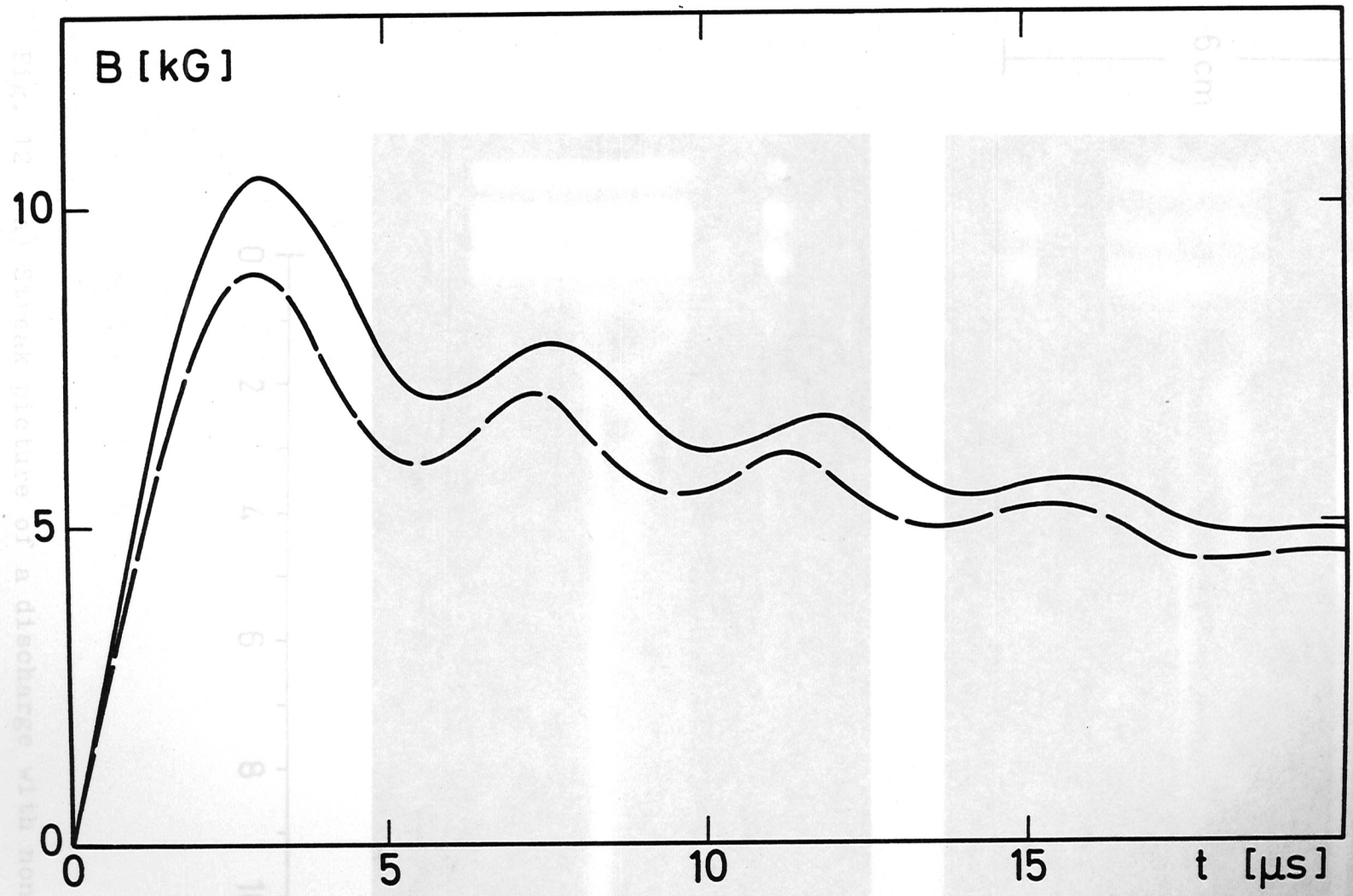

Fig. 11 Magnetic field of the main coil for R_o = 26 cm (solid curve), and magnetic field of the hexapole conductors for r_o = 3 cm between conductors (dashed curve). Main bank voltage 8 kV, hexapole bank voltage 10 kV.

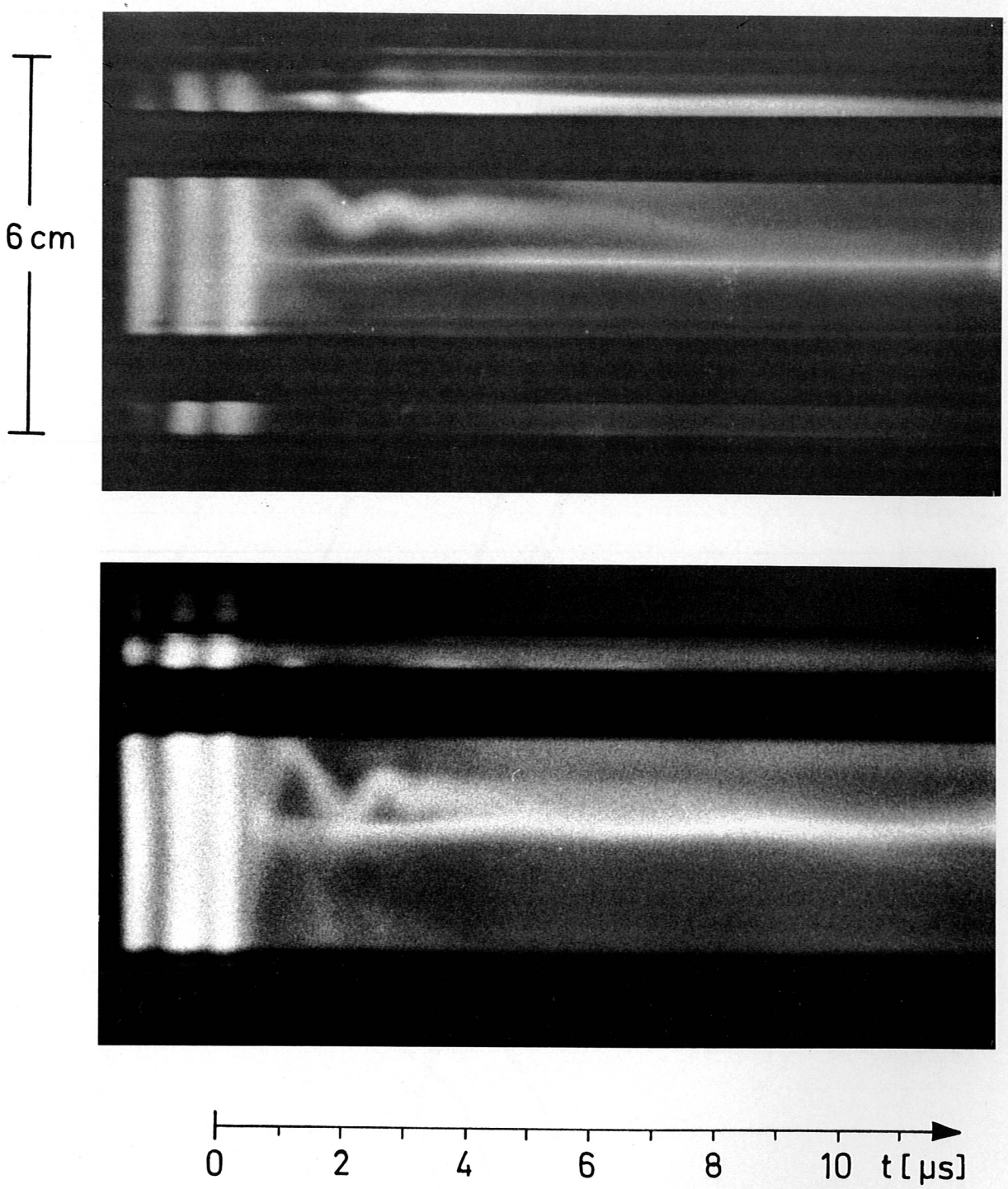

Fig. 12 a) Streak picture of a discharge with non-helical hexapole, n = 0;

b) the same for helical hexapole, n = 4/3.

Both are from experiment no.(5).

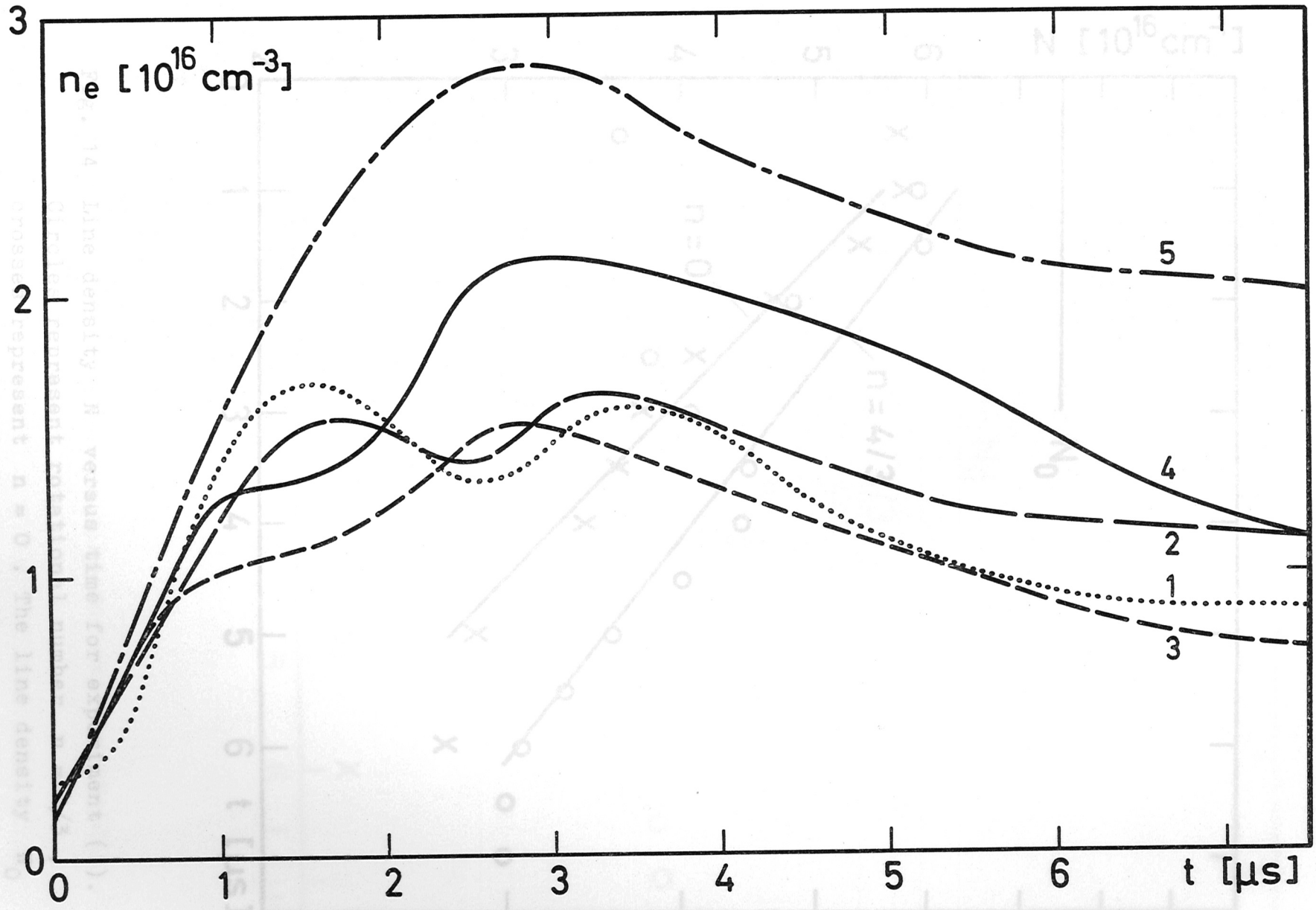

Fig. 13 Mean electron densities of experiments (1) to (5).

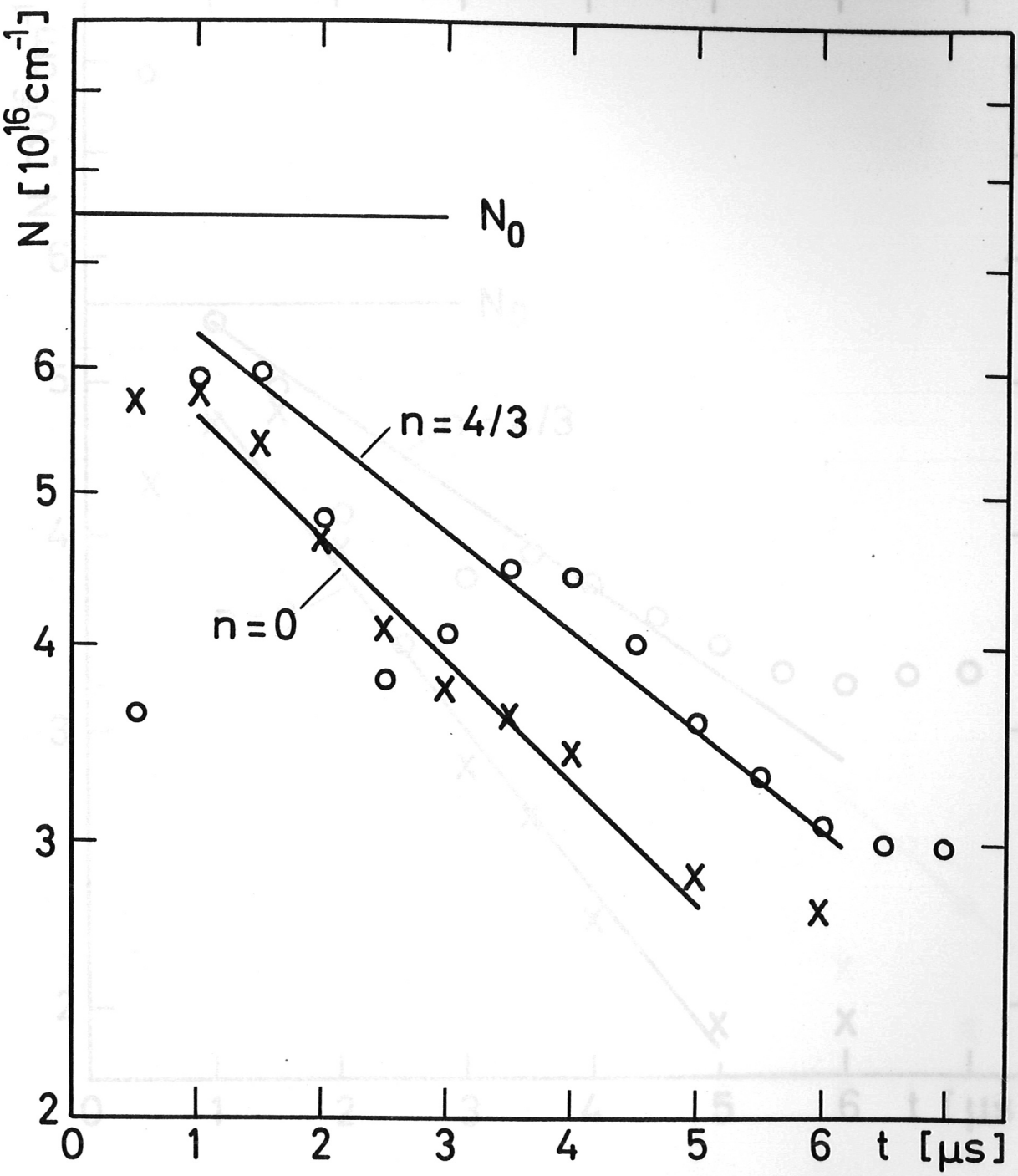

Fig. 14 Line density N versus time for experiment (1). Circles represent rotational number n = 4/3 , crosses represent n = 0 . The line density N_0 corresponds to a filling pressure of 40 mTorr.

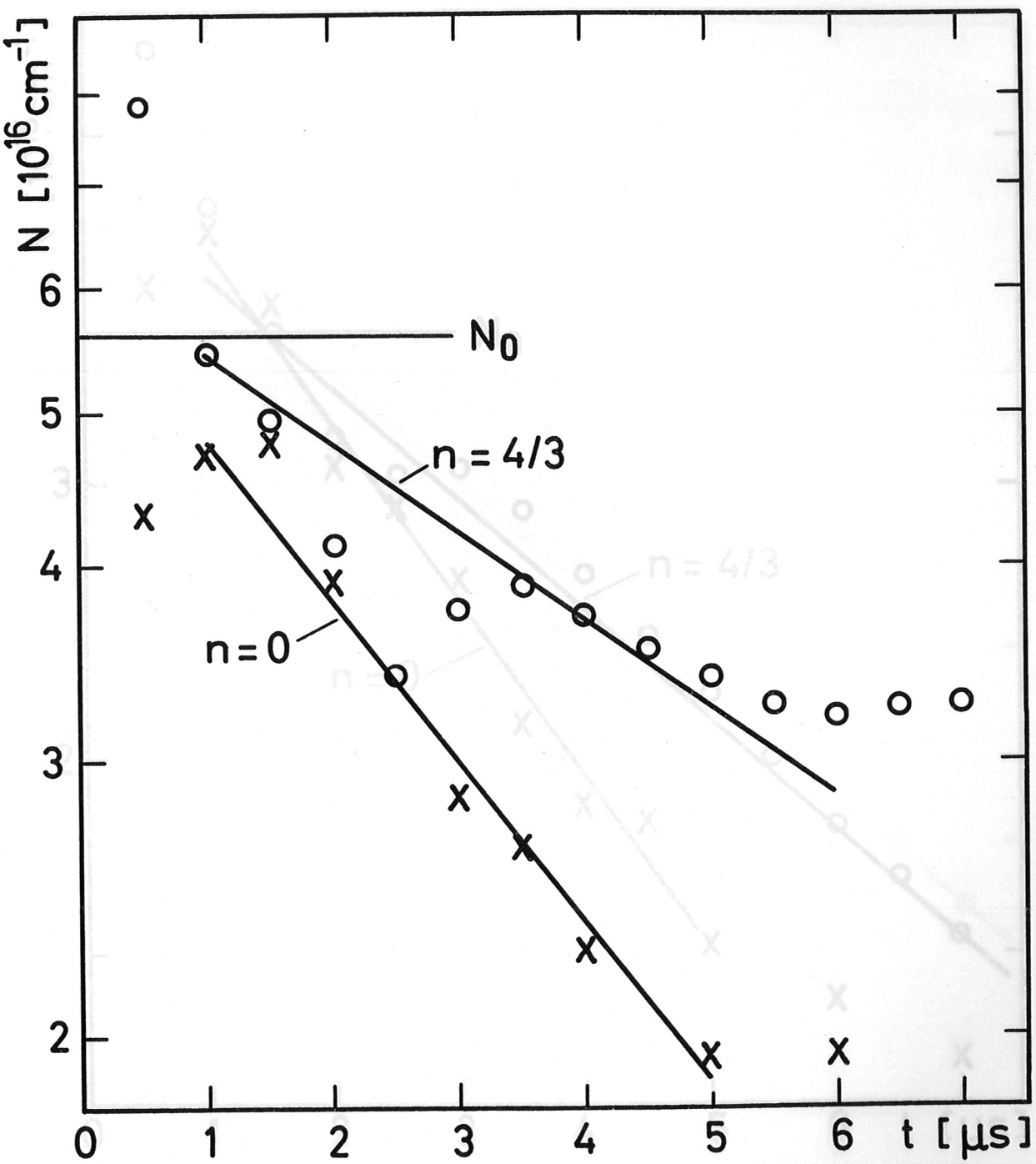

Fig. 15 Line density versus time for experiment (2).

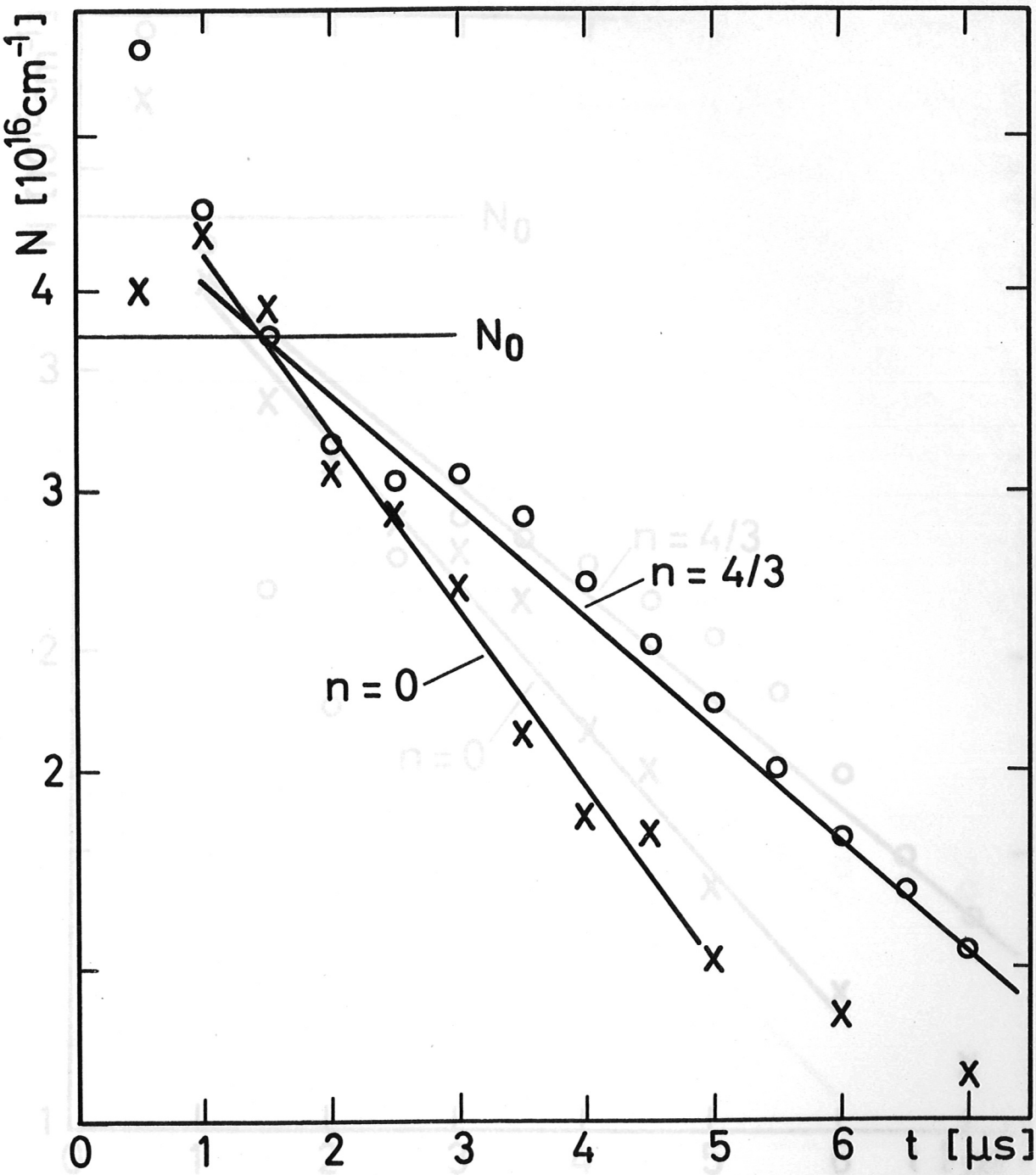

Fig. 16 Line density versus time for experiment (3).

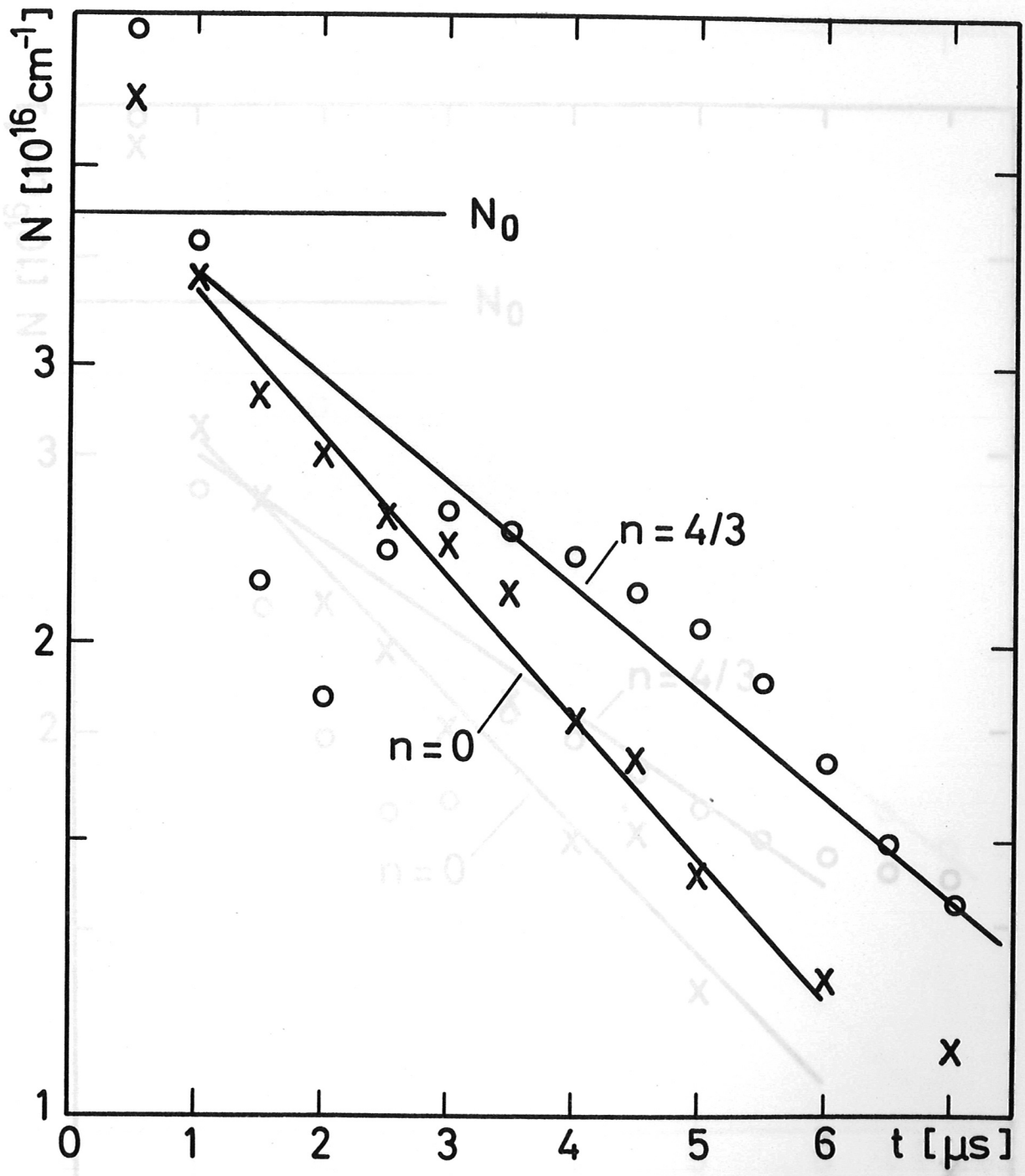

Fig. 17 Line density versus time for experiment (4).

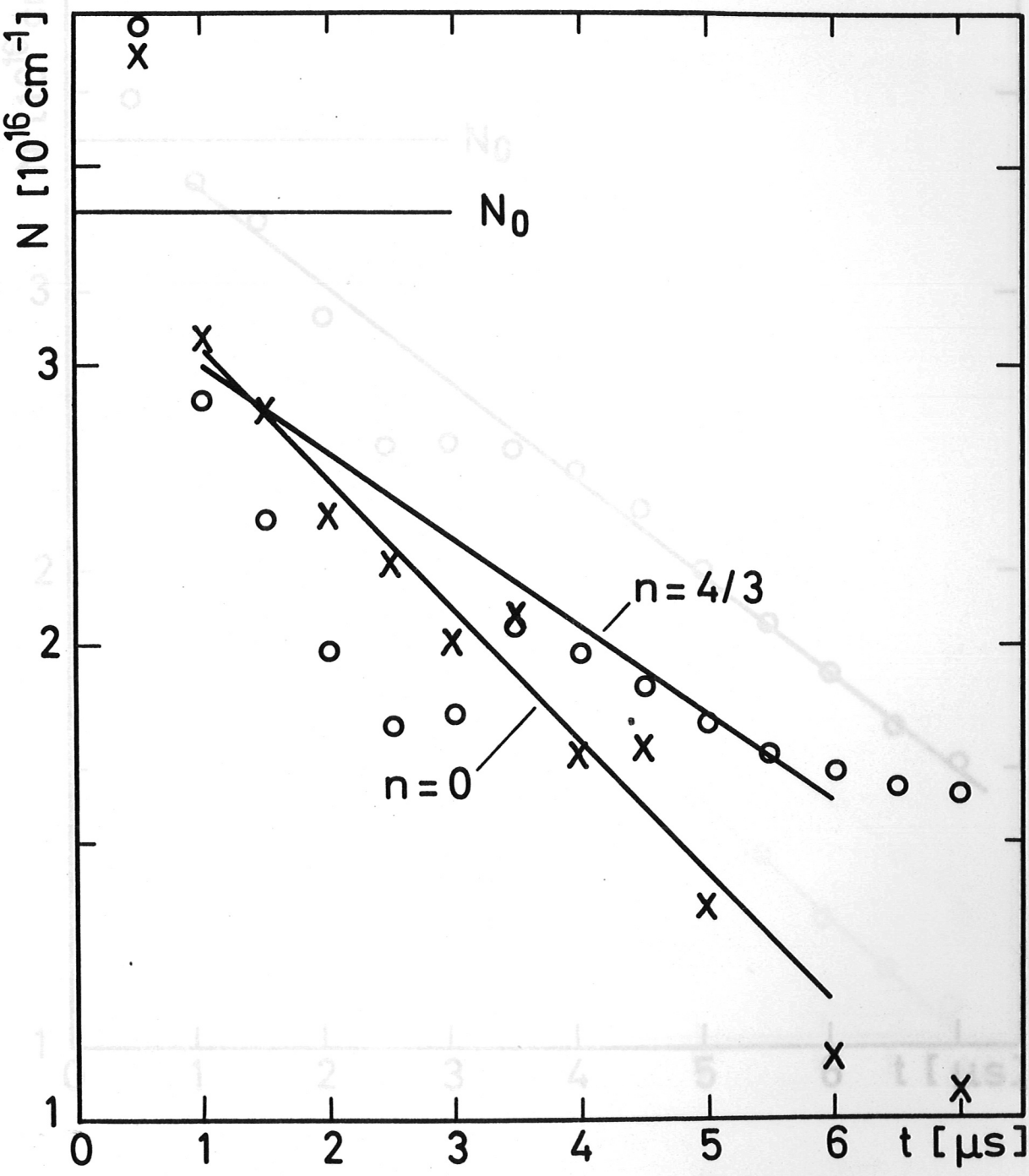

Fig. 18 Line density versus time for experiment (5).

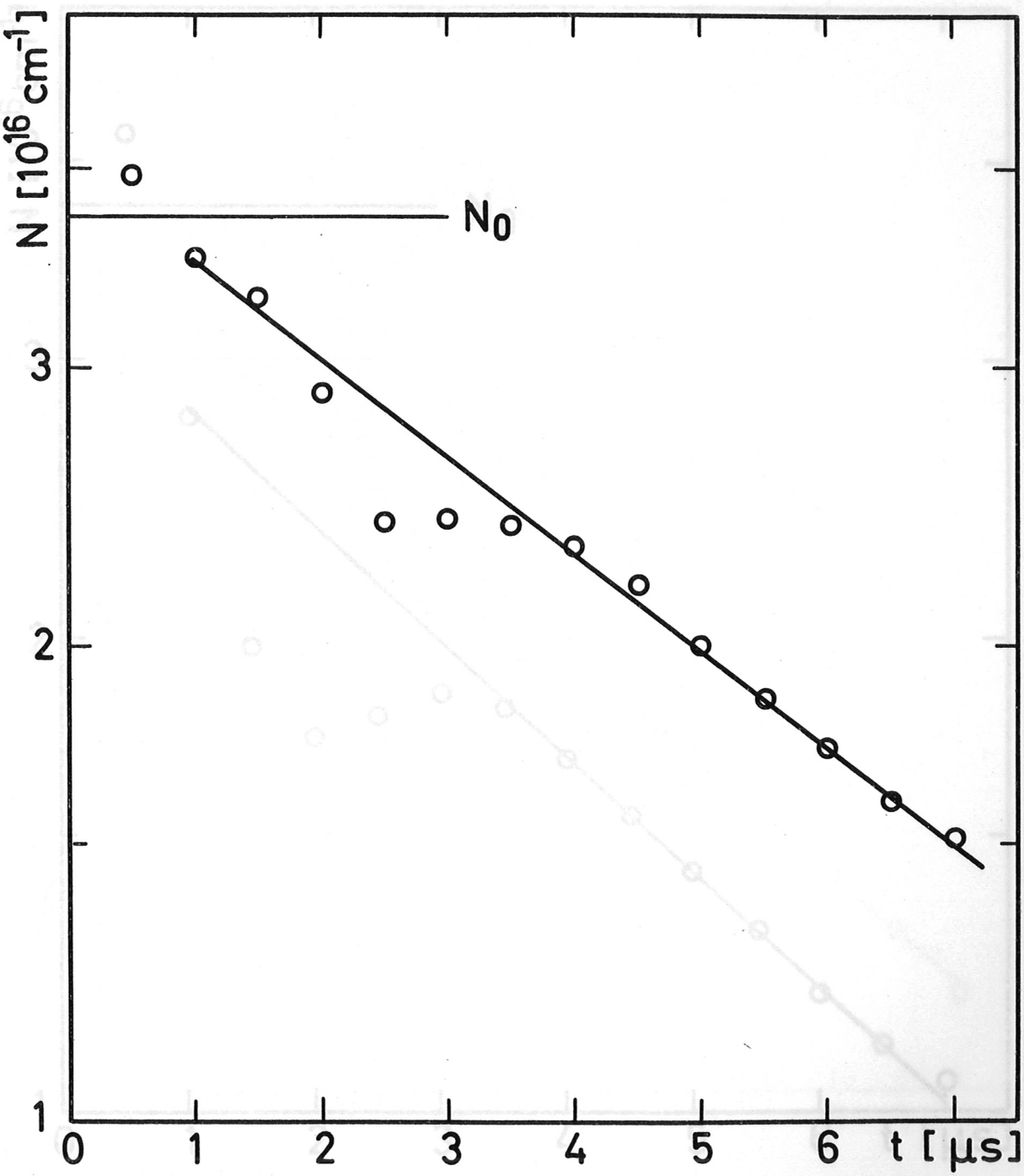

Fig. 19 Line density versus time for experiment (6).

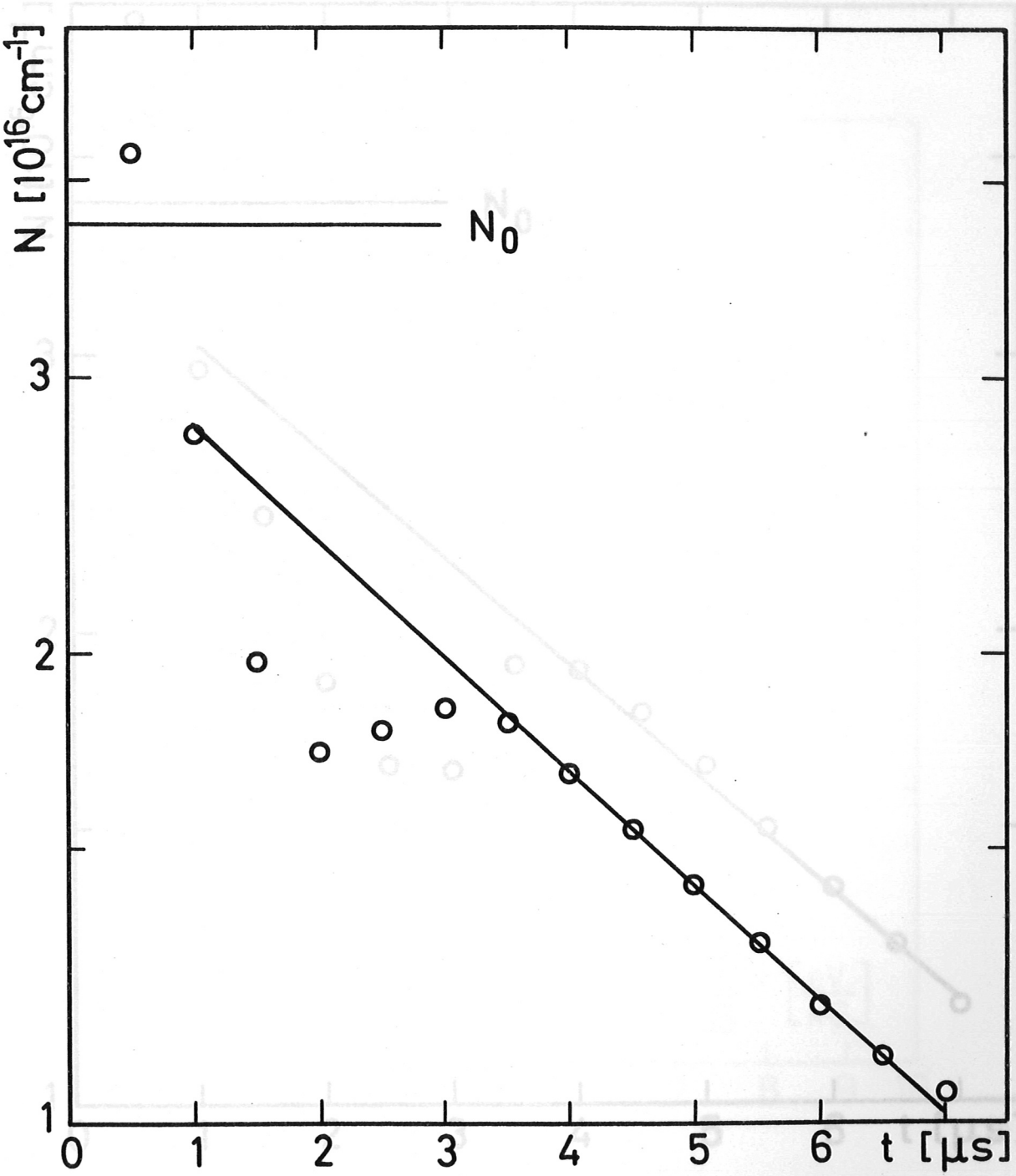

Fig. 20 Line density versus time for experiment (7).

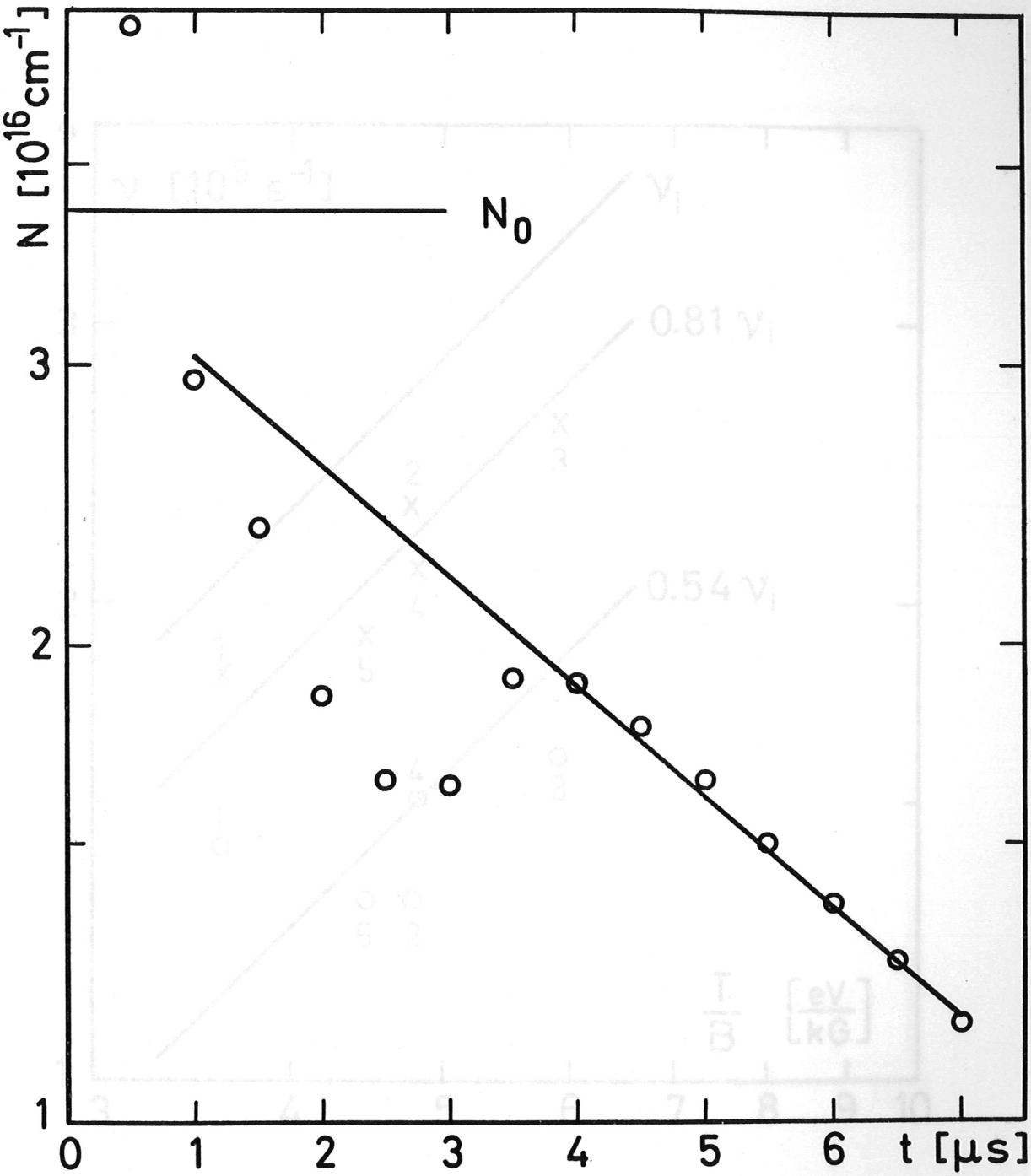

Fig. 21 Line density versus time for experiment (8).

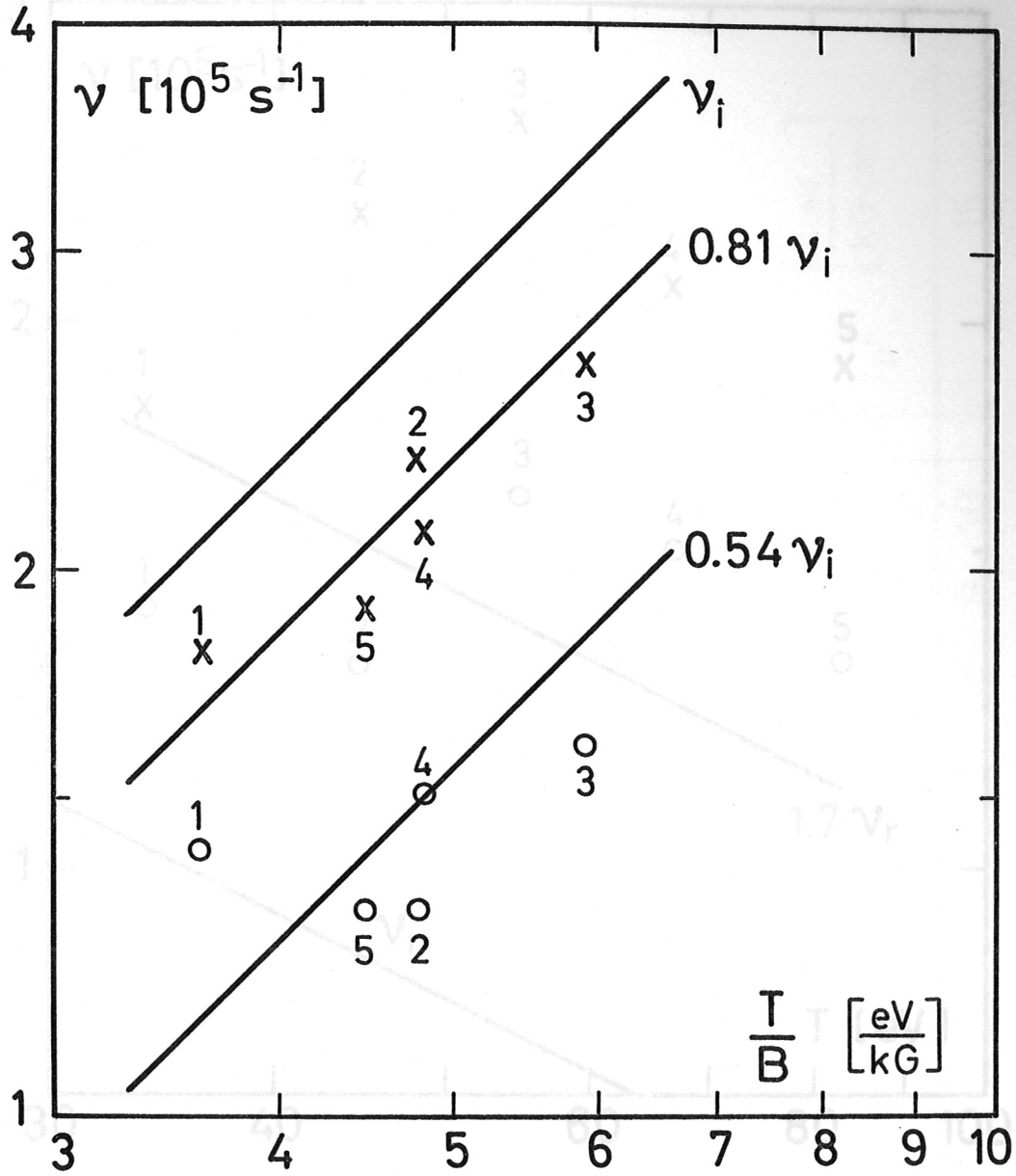

Fig. 22 Experiments compared with losses anticipated from cusp losses with a cusp slit width of one ion gyro radius. $\nu_i = 5.7 \times 10^4 \, (T/B) \, [s^{-1}]$, (T in eV; B in kG).
Circles represent n = 4/3, crosses represent n = 0.

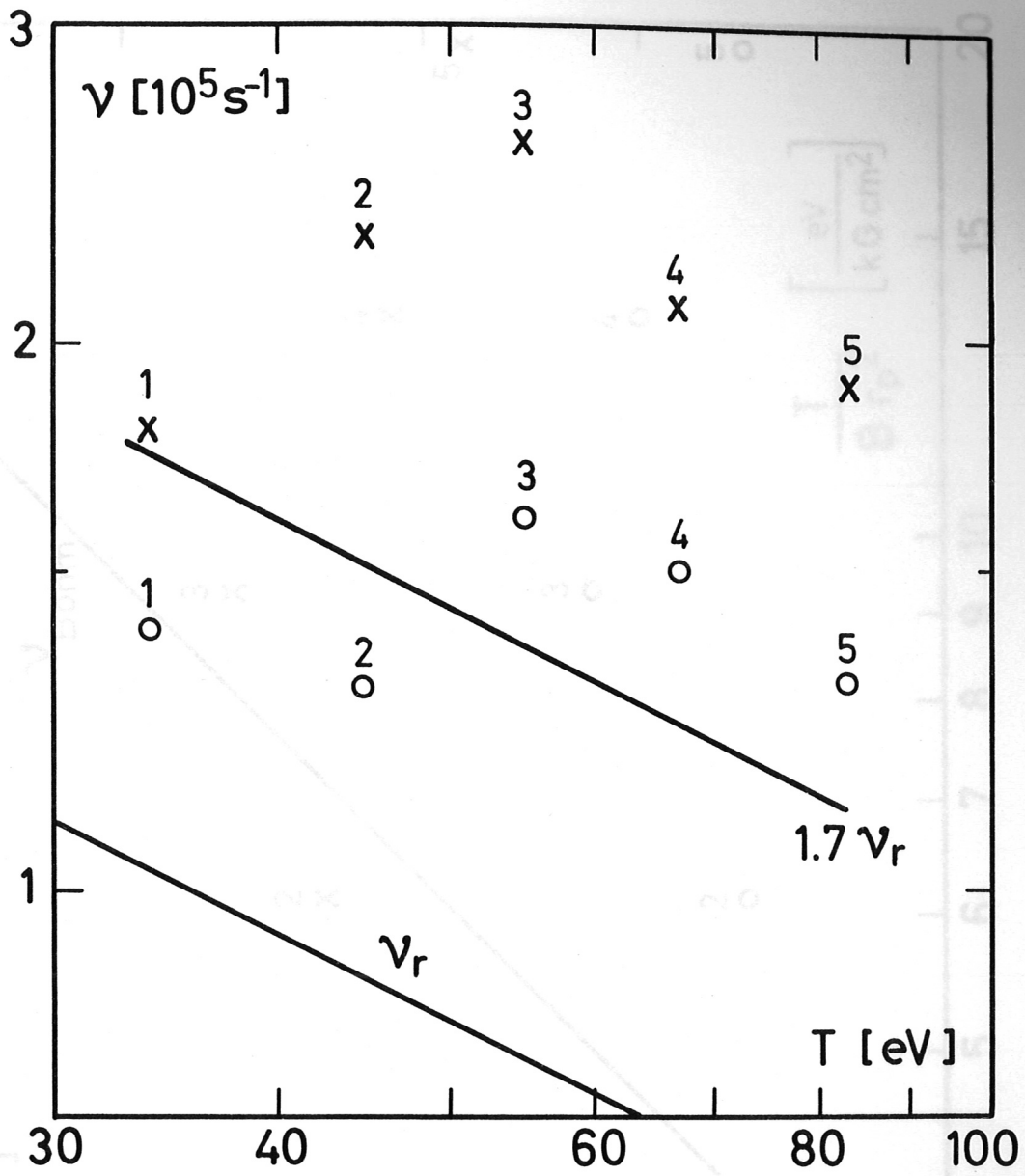

Fig. 23 Experiments compared with losses anticipated from classical diffusion $\nu_r = 6 \times 10^5 \, T^{-1/2} \, [s^{-1}]$, (T in eV).
Circles and crosses as in Fig. 22.

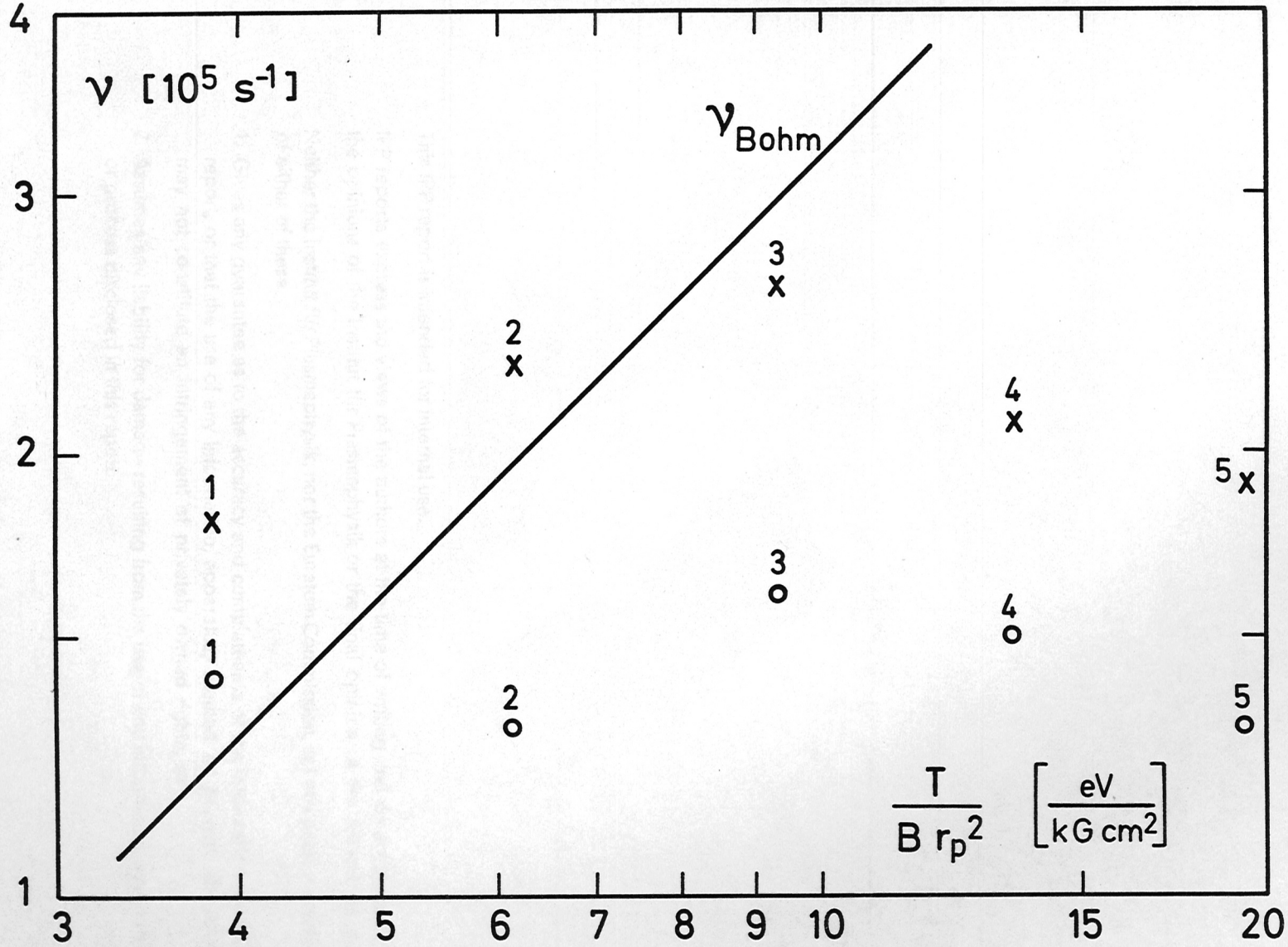

Fig. 24 Experiments compared with losses anticipated from Bohm diffusion, $\nu_{Bohm} = 3.2 \times 10^4 (T/B\, r_p^2)\ [s^{-1}]$, (T in eV; B in kG; r_p in cm). Circles and crosses as in Fig. 22.